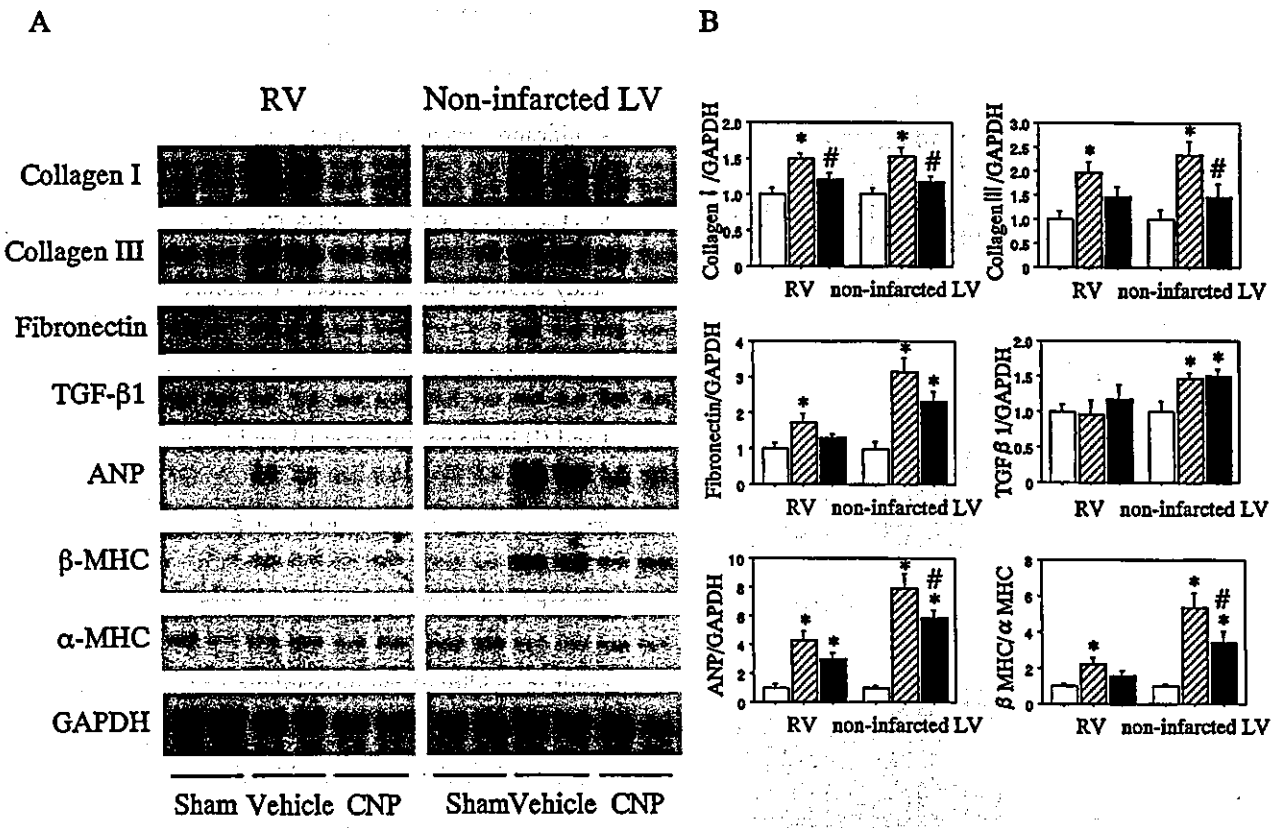

Figure 4. The effect of C-type natriuretic peptide (CNP) on messenger ribonucleic acid (mRNA) expression associated with cardiac remodeling after myocardial infarction (MI). (A) Typical autoradiograms of Northern blot analysis of mRNA levels in right ventricle (RV) and noninfarcted left ventricle (LV) for collagen type I, collagen type III, fibronectin, transforming growth factor-(TGF)-β-1, atrial natriuretic peptide (ANP), β- and α-myosin heavy chain (MHC), and glyceraldehyde-3-phosphate dehydrogenase (GAPDH) at the 18th day after MI. (B) Quantitative analyses of the abundance of each gene in the RV and noninfarcted LV at the 18th day after MI (n = 10 in each group). In individual samples, each mRNA value was corrected for the GAPDH mRNA value. Levels in sham-operated rats were arbitrarily assigned a value of 1.0. Values are mean ± SEM. $^{**}p < 0.01$, $^{*}p < 0.05$ compared with the sham-operated group; $\#p < 0.05$ compared with the MI+vehicle group by analysis of variance and Bonferroni multiple-comparison *t* test. Open bars = sham; striped bars = MI+vehicle; solid bars = MI+CNP.

parameters in the infarcted LV between the two MI groups (data not shown).

Cellular mechanism of the antifibrotic action of CNP. C-type natriuretic peptide and 8-Bromo cGMP, an analog of cGMP, decreased the incorporation of [^{3}H]proline into cardiac fibroblasts in a dose-dependent manner (Figs. 5A and 5B). The decrease of [^{3}H]proline incorporation by CNP was completely blocked by Rp-8-pCPT-cGMP, a cell-permeable inhibitor of PKG type I and type II, at a concentration of 10^{-5} mol/l (Fig. 5C).

Endogenous CNP expression after MI. C-type natriuretic peptide mRNA expression increased on day 3 by about four-fold in the infarcted LV and two-fold in the noninfarcted LV compared with sham rats, and gradually decreased from day 7 to day 18 (Fig. 6A). C-type natriuretic peptide mRNA expression in RV slightly increased on day 7 only (1.5-fold) (Fig. 6A). In addition, immunohistochemical study revealed that CNP was stained mainly in fibrotic area of the infarct and border region on day 7 after MI (Fig. 6B). These results suggest that endogenous local CNP might play an important role in the infarcted heart.

DISCUSSION

In this study, we have demonstrated that in vivo administration of CNP improved cardiac function and protected against cardiac remodeling after MI in rats. The beneficial effects of CNP treatment in the heart after MI included attenuation of cardiac fibrosis, hypertrophy, and LV enlargement.

In addition, continuous treatment with CNP had no effects on mean arterial pressure and LV systolic pressure at the time of sacrifice 18 days after MI. The serial change in noninvasive blood pressure during the recovery period after MI was also similar in rats with and without CNP treatment. These findings are consistent with previous studies, which showed that CNP infusion had little vasodepressor or natriuretic activities in rats and healthy humans (4,11).

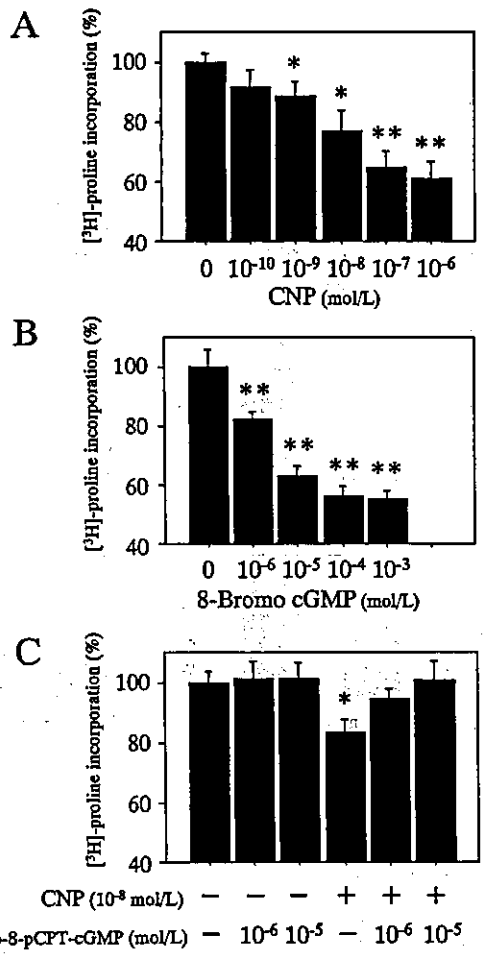

Figure 5. The effect of C-type natriuretic peptide (CNP) on collagen synthesis via the cyclic guanosine monophosphate (cGMP)/cyclic guanosine monophosphate-dependent protein kinase (PKG) pathway in cultured neonatal rat cardiac fibroblasts. **(A and B)** The effect of CNP and 8-Bromo cGMP on [^{3}H]proline incorporation in cardiac fibroblasts. **(C)** [^{3}H]proline incorporation in the presence or absence of 10^{-8} mol/l CNP with or without Rp-8-pCPT-cGMP, PKG inhibitor. Values are mean ± SEM. $^{**}p < 0.01$, $^{*}p < 0.05$ compared with control by analysis of variance and Bonferroni multiple-comparison *t* test.

Similarly, the heart rate was not significantly affected by CNP infusion throughout the study period.

The effect of CNP on cardiac performance. Chronic administration of CNP improved cardiac performance in MI rats, as indicated by increases in LV fractional shortening, cardiac output, and LV $dP/dt_{max/min}$, and by decreases in E/A ratio and LV end-diastolic pressure, which were accompanied by improvement of LV enlargement. Because the effect of CNP on pre- or after-load, heart rate, and infarct size was very little, a mechanism other than hemodynamic improvement or reduction in infarct size is probably the cause of the beneficial effects of CNP on cardiac performance.

The beneficial effect of CNP on cardiac remodeling through its antifibrotic action. One possibility is that CNP directly inhibits myocardial fibrosis because we have previously demonstrated that CNP directly inhibited both DNA and collagen synthesis by cardiac fibroblasts in vitro (6). In the present study, we have, therefore, examined the in vivo effect of CNP on fibrosis and found that CNP significantly attenuated an increase in morphometrical collagen volume fraction in the noninfarcted LV and RV. In addition, the effect of CNP was more prominent in the border region of MI, in which fibrosis was more increased, than that in the remote region. Because our preliminary study showed that a number of fibroblasts shift toward a myofibroblastic phenotype indicated by α-smooth muscle actin in the border region of MI, CNP might have more potent inhibitory effect on myofibroblast-like cells than on fibroblasts. Furthermore, the mRNA levels of collagen type I and III in the noninfarcted LV and RV were suppressed by treatment with CNP. These results provide in vivo evidence that CNP is a potent "fibrosis-inhibitory agent" after MI. The amount of myocardial collagen deposition in the infarcted and noninfarcted regions during healing after MI was reported to influence and to be integral to the process of ventricular remodeling (16). In addition, it has been shown that excessive accumulation of myocardial collagen might result in rigidity of the myocardium and severely impaired relaxation (17). Therefore, improved LV $dP/dt_{max/min}$ by CNP after MI might reflect improved myocardial rigidity in the noninfarcted region caused by the reduction in cardiac fibrosis.

Given the in vivo antifibrotic action of CNP, we further explored the cellular mechanisms of this action in vitro. Consistent with our previous study (6), CNP or 8-Bromo cGMP, an analog of cGMP, potently inhibited collagen synthesis of cultured cardiac fibroblasts. In the present study, the inhibitory effect of CNP was completely blocked by Rp-8-pCPT-cGMP, an inhibitor of PKG (Fig. 5), indicating that CNP inhibited collagen synthesis by activating cGMP/PKG pathway.

Some experimental data suggest that antifibrotic agents could potentially enhance the remodeling of the extracellular collagen matrix in the infarct zone during very early stage of healing after MI (18). However, in the present study, the death rate of the MI+CNP group (6%) was lower than that of the MI+vehicle group (17%) during the two-week infusion period, and two dead rats with CNP treatment showed no findings of LV rupture. The late start of CNP infusion at the fourth day of MI might reduce the potential adverse effects of antifibrosis such as wall thinning of infarct zone. Further studies are needed to determine the best timing of CNP treatment after MI.

The beneficial effect of CNP on cardiac remodeling through its antihypertrophic action. Another possible mechanism of cardioprotection by CNP might be attenuated myocardial hypertrophy after MI. As shown in the Results section, CNP effectively reduced the MI-induced myocardial hypertrophy in vivo. The findings are in agreement with previous in vitro studies, which showed that natriuretic peptides including CNP prevented hypertrophy

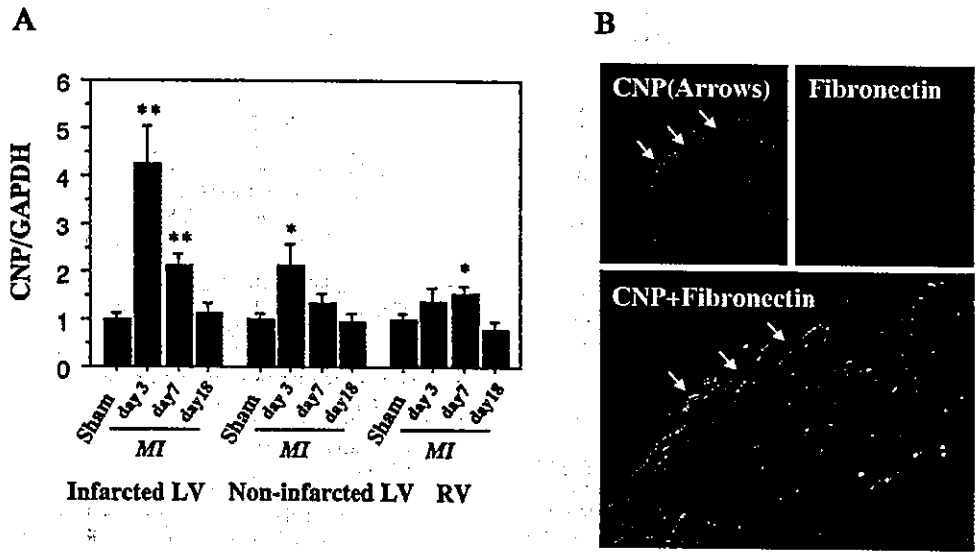

Figure 6. Endogenous C-type natriuretic peptide (CNP) expressions after myocardial infarction (MI). **(A)** Endogenous CNP mRNA abundance in the infarcted left ventricle (LV), noninfarcted LV, and right ventricle (RV) at different times after MI and on day 3 after sham operation. Values are mean ± SEM. $^{**}p < 0.01$, $^{*}p < 0.05$ compared with sham by analysis of variance and Bonferroni's multiple-comparison *t* test. **(B)** Immunofluorescent microscopic CNP expression. Upper photomicrographs show the section on day 7 after MI stained by the specific antibody against CNP-53 **(left, green)** and stained by antifibronectin antibody **(right, red)**. Lower photomicrograph shows the merged image (×600 magnification). GAPDH = glyceraldehydes-3-phosphate dehydrogenase.

of cultured cardiomyocytes (7,19). Although the precise mechanism by which CNP inhibits cardiac hypertrophy remains unknown, our previous study (7) suggested that CNP inhibits hypertrophy of cardiac myocytes directly by activating cGMP-dependent mechanism and indirectly by reducing endothelin-1 secretion from nonmyocytes.

On the other hand, because hypertrophy after MI is an adaptive response that offsets increased load, attenuates progressive dilation, and stabilizes contractile function (20), decreased cardiac hypertrophy shown in the present study might be caused by the indirect effect of CNP via decreased LV systolic wall stress. Further studies are needed to determine the contribution ratio of direct and indirect effects of CNP on cardiac hypertrophy.

Comparison with other antiremodeling therapies after MI. A number of therapeutic approaches to limiting ventricular remodeling in MI have been reported. These agents include angiotensin-converting enzyme inhibitors, angiotensin II type 1 receptor blockers, β-adrenergic blockers, aldosterone antagonists, and matrix metalloproteinase inhibitors. Although a number of these other agents have been given orally and, in this regard, they have an advantage over CNP, CNP treatment has some advantages concerning short treatment period and fewer side effects. Actually, in previous studies, it took more than four weeks for other agents to attain similar reduction of collagen volume fraction as two weeks treatment of CNP. Furthermore, these synthetic agents might cause harmful effects such as severe hypotension by vasodilators (21) or musculoskeletal toxicity by matrix metalloproteinase inhibitors (22). Because CNP does not affect blood pressure, it can be used in hemodynamically unstable patients as often seen in acute MI.

Study limitations. Because the effects of CNP were evaluated after two weeks of therapy in the present study, its long-term effects on the cardiac remodeling after MI remain unclear. For future clinical application, further study is necessary to examine if the antiremodeling effects of CNP persist for the long-term follow-up period.

Summary. Our study has demonstrated that continuous administration of CNP improved LV dysfunction and attenuated the development of cardiac remodeling after MI. Because CNP has much weaker vasorelaxant and natriuretic activities, but has much more potent antifibrotic and antihypertrophic actions than ANP or BNP, these beneficial effects of CNP might be associated with direct effects on the failing heart. In conclusion, CNP is potentially useful as a new antiremodeling agent through its novel mechanism of action.

Acknowledgments

The authors are grateful to Dr. Yujiro Hayashi, Daiichi Suntory Pharma, for the kind gift of CNP. We also thank Ms. Chika Fukuhara for her excellent technical assistance.

Reprint requests and correspondence: Dr. Ichiro Kishimoto, Department of Biochemistry, National Cardiovascular Center Research Institute, 5-7-1 Fujishiro-dai, Suita, Osaka 565-8565, Japan. E-mail: kishimot@ri.ncvc.go.jp.

REFERENCES

1. Rosenzweig A, Seidman CE. Atrial natriuretic factor and related peptide hormones. Annu Rev Biochem 1991;60:229–55.
2. Levin ER, Gardner DG, Samson WK. Natriuretic peptides. N Engl J Med 1998;339:321–8.

3. Nakao K, Ogawa Y, Suga S, et al. Molecular biology and biochemistry of the natriuretic peptide system. I: Natriuretic peptides. J Hypertens 1992;10:907–12.
4. Sudoh T, Minamino N, Kangawa K, Matsuo H. C-type natriuretic peptide (CNP): a new member of natriuretic peptide family identified in porcine brain. Biochem Biophys Res Commun 1990;168:863–70.
5. Furuya M, Miyazaki T, Honbou N, et al. C-type natriuretic peptide inhibits intimal thickening after vascular injury. Ann NY Acad Sci 1995;748:517–23.
6. Horio T, Tokudome T, Maki T, et al. Gene expression, secretion, and autocrine action of C-type natriuretic peptide in cultured adult rat cardiac fibroblasts. Endocrinology 2003;144:2279–84.
7. Tokudome T, Horio T, Soeki T, et al. Inhibitory effect of C-type natriuretic peptide (CNP) on cultured cardiac myocyte hypertrophy: interference between CNP and endothelin-1 signaling pathways. Endocrinology 2004;145:2131–40.
8. Kalra PR, Clague JR, Bolger AP, et al. Myocardial production of C-type natriuretic peptide in chronic heart failure. Circulation 2003; 107:571–3.
9. Hammermeister KE, DeRouen TA, Dodge HT. Variables predictive of survival in patients with coronary artery disease: selection by univariate and multivariate analysis from the clinical, electrocardiographic, exercise, arteriographic, and quantitative angiographic evaluations. Circulation 1979;59:421–30.
10. Sutton MG, Sharpe N. Left ventricular remodeling after myocardial infarction: pathophysiology and therapy. Circulation 2000;101: 2981–8.
11. Igaki T, Itoh H, Suga SI, et al. Effects of intravenously administered C-type natriuretic peptide in humans: comparison with atrial natriuretic peptide. Hypertens Res 1998;21:7–13.
12. Nagaya N, Uematsu M, Kojima M, et al. Chronic administration of ghrelin improves left ventricular dysfunction and attenuates development of cardiac cachexia in rats with heart failure. Circulation 2001;104:1430–5.
13. Fishbein MC, Maclean D, Maroko PR. Experimental myocardial infarction in the rat: qualitative and quantitative changes during pathologic evolution. Am J Pathol 1978;90:57–70.
14. Horio T, Nishikimi T, Yoshihara F, et al. Production and secretion of adrenomedullin in cultured rat cardiac myocytes and nonmyocytes: stimulation by interleukin-1 beta and tumor necrosis factor-alpha. Endocrinology 1998;139:4576–80.
15. Thompson NL, Bazoberry F, Speir EH, et al. Transforming growth factor beta-1 in acute myocardial infarction in rats. Growth Factors 1988;1:91–9.
16. Jugdutt BI, Joljart MJ, Khan MI. Rate of collagen deposition during healing and ventricular remodeling after myocardial infarction in rat and dog models. Circulation 1996;94:94–101.
17. Doering CW, Jalil JE, Janicki JS, et al. Collagen network remodelling and diastolic stiffness of the rat left ventricle with pressure overload hypertrophy. Cardiovasc Res 1988;22:686–95.
18. Jugdutt BI. Ventricular remodeling after infarction and the extracellular collagen matrix: when is enough enough? Circulation 2003;108: 1395–403.
19. Rosenkranz AC, Woods RL, Dusting GJ, Ritchie RH. Antihypertrophic actions of the natriuretic peptides in adult rat cardiomyocytes: importance of cyclic GMP. Cardiovasc Res 2003;57:515–22.
20. Pfeffer MA, Braunwald E. Ventricular remodeling after myocardial infarction. Experimental observations and clinical implications. Circulation 1990;81:1161–72.
21. Jugdutt BI. Myocardial salvage by intravenous nitroglycerin in conscious dogs: loss of beneficial effect with marked nitroglycerin-induced hypotension. Circulation 1983;68:673–84.
22. Drummond AH, Beckett P, Brown PD, et al. Preclinical and clinical studies of MMP inhibitors in cancer. Ann NY Acad Sci 1999;878: 228–35.

Endocrine Journal 2004, **51** (6), 569–577

Identification of 2,3,7,8-Tetrachlorodibenzo-p-dioxin (TCDD)-inducible and -suppressive Genes in the Rat Placenta: Induction of Interferon-regulated Genes with Possible Inhibitory Roles for Angiogenesis in the Placenta

TETSUYA MIZUTANI, MIKI YOSHINO, TOMOKO SATAKE, MIYUKI NAKAGAWA, RYUTA ISHIMURA*, CHIHARU TOHYAMA*, KOICHI KOKAME**, KENJI KANGAWA** AND KAORU MIYAMOTO

Department of Biochemistry, Faculty of Medical Sciences, University of Fukui, Matsuoka, Fukui 910-1193, Japan; CREST, JST, Kawaguchi 332-0012, Japan

**Environmental Health Sciences Division, and Endocrine Disruptors and Dioxin Research Project, National Institute for Environmental Studies, 16-2 Onogawa, Tsukuba 305-8506, Japan; CREST, JST, Kawaguchi 332-0012, Japan*

***National Cardiovascular Center Research Institute, 5-7-1 Fujishirodai, Suita, Osaka 565-8565, Japan*

Abstract. Exposure to a low dose of 2,3,7,8-tetrachlorodibenzo-p-dioxin (TCDD) results in a variety of toxic manifestations, including fetal death. In order to evaluate the effects of low dose TCDD on placental function, pregnant Holtzman rats were given a single oral dose of 1600 ng TCDD/kg body wt or an equivalent volume of vehicle (control) on gestation day 15 (GD15), and changes in the gene expression in the placenta on GD20 were analyzed by two comprehensive methods, representational difference analysis (RDA) and DNA microarray technology. Candidates of TCDD-inducible and -suppressive genes were selected. Quantitative real-time PCR analysis was then performed to verify the induction or suppression levels of the candidate genes. Finally, we identified 81 TCDD-inducible and 21 TCDD-suppressive genes from the placenta of TCDD-treated Holtzman rats on GD20. One of the remarkable profiles of the gene expression was that glucose transporters were strongly up-regulated by the TCDD treatment. Furthermore, many interferon-inducible genes were also up-regulated by the treatment. They included several cytokines such as IP-10 known as a potent angiogenesis inhibitor. In addition, interferon molecules are known to suppress angiogenesis. The above observations suggest that activation of the interferon signaling pathway and the induction of anti-angiogenic factors by TCDD might have a role in causing the inhibition of neovascularization, resulting in the hypoxic state of placenta and increased incidence of fetal death.

Key words: TCDD, Placenta, Gene expression, Real-time PCR, DNA microarray

(*Endocrine Journal* **51**: 569–577, 2004)

2,3,7,8-Tetrachlorodibenzo-p-dioxin (TCDD) is known to be the most toxic congener among the dioxin and related compounds found in the environment. Exposure to TCDD causes a diverse spectrum of toxicities in humans and laboratory animals [1–4]. The fetus is one of the most sensitive targets of TCDD and exhibits a wide range of biological responses at low TCDD levels that have no detectable effects on maternal side (usually the levels were ten to hundred times lower than those of LD50). One of the most severe adverse effects of TCDD is intrauterine fetal death [1, 5–7]. The incidence has been shown in all species studied to date, including the monkey, hamster, rat, and mouse. Although fetal death is an important aspect of TCDD toxicity, its precise mechanism is not well understood. Placenta plays a crucial role in maintaining normal fetal growth such as exchange of oxygen and carbohydrate nutrients. In previous studies Ishimura *et al.*

Received: May 28, 2004
Accepted: October 5, 2004
Correspondence to: Dr. Kaoru MIYAMOTO, Department of Biochemistry, Faculty of Medical Sciences, University of Fukui, Matsuoka, Fukui 910-1193, Japan

demonstrated that exposure of pregnant rats to 800 or 1600 ng TCDD/kg on gestational day 15 (GD15) resulted in an increased incidence of fetal death on GD20 [8, 9]. In their experimental protocol, the placenta showed several abnormalities that led to increased risk for fetal death. Exposure to TCDD altered the glucose kinetics in placenta [8] and caused reduced blood flow and placental hypoxia [9], leading them to hypothesize that the increased incidence of the fetal death may be due to reduced blood flow into the placenta [8, 9]. In order to clarify what kind of genes are involved in these placental abnormalities or what other aspects of TCDD toxicities exist in the placenta, we conducted a comprehensive analysis of gene expression in placenta of pregnant Holtzman rats treated with TCDD using representational difference analysis (RDA) and DNA microarray technology. RDA is a subtraction cloning method developed by Pastorian *et al.* [10]. The RDA and the DNA microarray are very powerful and comprehensive methods to identify inducible or suppressive genes by given hormonal or pharmacological treatments. Previously we have reported many gonadotropin-inducible genes in the rat ovary by using those methods [11–13]. In this study, many candidates for placental TCDD-inducible or -suppressive genes were selected by those methods, and the induction or suppression was verified by quantitative real-time PCR.

Profiling analysis of the verified genes revealed that, in addition to the genes involved in the glucose uptake, those involved in the interferon signaling pathway were strongly induced by the TCDD treatment. Based on the results obtained, the molecular mechanisms of placental disorders by low dose TCDD will be discussed.

Materials and Methods

Reagents

2,3,7,8-TCDD was obtained from Cambridge Isotope Laboratory (Andover, MA). Rat cDNA glass array (Gene Chip Rat Expression Array 230A) was from Affymetrix, Inc., Santa Clara, CA.

Animals

Holtzman rats were purchased from Harlan Sprague-Dawley (Indianapolis, IN). The animals were maintained in a controlled environment with 12/12 h light/dark cycles, and given free access to laboratory rat chow and water. Female rats were allowed to mate on proestrus overnight, and, if vaginal plugs were observed in the morning, the day was designated GD0. Six pregnant rats were treated with TCDD, and a total of 10 dead fetuses was observed among 83 fetuses. The pregnant rats were housed individually until exercised. All animal experiments were performed according to the guidelines for animal welfare of the National Institute for Environmental Studies [8, 9].

TCDD treatment

The pregnant animals were exposed to TCDD as described previously [8, 9]. TCDD was dissolved in nonane at a concentration of 20 μg/ml, and the solution was diluted with corn oil. On GD15 the pregnant rats were given a single oral dose of 1600 ng TCDD/kg body wt or an equivalent volume of mixture of nonane and corn oil solution (control). Placentas were collected from the TCDD treated or control rats on GD20. The placental samples were immediately frozen in liquid nitrogen and maintained at –80°C until used.

Representational difference analysis

For isolating TCDD-inducible and -suppressive genes from the placenta, representational difference analysis (RDA) was performed according to the procedure reported by Pastorian *et al.* [10]. Briefly, total RNA was extracted from each placenta. Each five placental RNA samples were mixed and used for further analysis. After Oligo-dT latex beads treatment, mRNA preparations were then converted to respective double-stranded cDNAs. Tester TCDD-treated placental cDNAs and driver control placental cDNAs were digested with a restriction enzyme DpnII. The digested tester cDNA fragments were ligated with first-round adaptor oligonucleotide molecules, and then mixed with the excess amount of the enzyme digested driver cDNAs. The mixture was denatured and then incubated at 67°C for 16 hours for hybridization. After the hybridization, only the tester specific cDNA fragments were amplified by PCR reaction using primers complementary to the adaptor sequence. For the second cycle RDA, the resulting PCR products, in which the tester specific cDNA fragments were enriched, were digested again with DpnII, and then followed by the second adaptor

ligation and hybridization in order to further enrich tester specific cDNA fragments. The PCR products after the second RDA reaction were ligated in to pGEM T-vector, and individual clones were analyzed to identify TCDD-sensitive genes.

DNA microarray

The microarray method was carried out according to the manufacturer's instruction.

Briefly, total RNA was extracted from the TCDD-treated and control placentas described above. Double stranded cDNA libraries were constructed from the mRNA of TCDD-treated and the control placentas using an oligo-dT primer with a T7-promoter sequence at the 5'-end. Biotin-labeled complementary RNA was *in vitro* transcribed by T7 polymerase using the cDNA libraries as template. The biotin-labeled RNA was fragmented and hybridized to the Rat cDNA glass array for 16 hr at 45°C and then washed and stained using the GeneChip Fluidics. The array was scanned by a GeneArray scanner, and hybridization patterns were detected as fluorescent light from reporter groups that have been incorporated into the target genes. The average difference measurements computed in the Affymetrix Microarray Analysis Suite 4.0 serve as a relative indicator of the level of expression.

Quantitative Real-Time PCR

Messenger RNA was extracted using an RNA extraction solution (Trizol) and oligo-dT latex beads as described previously [11–13]. Five micrograms of mRNA preparations were reverse-transcribed, and then converted to double stranded cDNA molecules. Complementary DNA was quantified by UV absorption measurement, and 1 ng was subjected to the PCR reaction as template. As an internal standard, TATA binding protein (TBP) was used instead of GAPDH, since GAPDH gene expression was affected by the TCDD treatment (data not shown). PCR reaction involved template cDNA samples, Advantage Taq Plus DNA polymerase (Clontech), dNTP, and Syber Green. Serial dilutions of the templates were used to create a concentration curve, and relative expression levels were calculated for each sample [14]. Abundance of each gene was referred to as a Ct (cycle threshold) value in this system.

Results

Exposure of pregnant Holtzman rats to 1600 ng TCDD/kg on GD15 resulted in an increased incidence of fetal death on GD20 [8, 9]. In these studies, each placenta from the TCDD-treated and control rats was prepared by the same exposure protocol as previous studies [8, 9], and gene expression in the placenta was analyzed by RDA and DNA microarray methods. Generally the RDA method is more sensitive than the DNA microarray, while the latter covers more comprehensive genes than the RDA method. A total of 2536 clones were picked-up and characterized from the RDA-subtracted cDNA libraries as candidate genes. In addition, the same tissues were used for the DNA-microarray, and among 13000 genes spotted on the array, 43 TCDD-inducible and 18 TCDD-suppressive candidate genes (cut-off values of 2.0 as inducible and 0.5 as suppressive genes) were also picked-up. All of these candidate genes picked-up by both methods were verified by using real-time PCR analysis, and genes that showed expression ratios (TCDD-treated/control) of more than 2.0 or less than 0.5 were finally identified as TCDD-sensitive. TCDD-inducible and -suppressive genes in the rat placenta identified by RDA and DNA microarray methods were summarized in Table 1 and Table 2, respectively.

TCDD-inducible genes in the placenta

As listed in Table 1, 81 genes were identified as TCDD-inducible genes in the placenta, 22 genes of which were from the results of DNA microarray analysis. Eleven genes were reported only on EST databases, and one gene showed no significant similarity to any gene on DNA databases. Other genes were all annotated as shown in Table 1 including those homologues of human or mouse. They were categorized into several groups. Enzyme genes include CYP1A1 and CYP1B1 that are known as the typical TCDD target genes [15, 16]. Inducible genes in placenta include some of the major blood proteins, such as prealbumin, apolipoproteins, transferrin, retinol-binding protein, prothrombin, and fibrinogens. This suggests that the placental production of the blood proteins was stimulated by the TCDD treatment. In addition, two placental specific genes, alpha-fetoprotein and pregnancy-specific glycoprotein (rnCGM3), were also induced by the TCDD treatment.

Table 1. TCDD-inducible genes in the rat placenta

Molecular function	Description	Array ratio	Real Time PCR ratio	Ct	Accession
Enzyme	(LMW) K-kininogen	3.32	8.14	30.06	M11884
	(LMW) T-kininogen I	ND	4.43	30.53	M11883
	Aldolase B	ND	2.72	34.15	M10149
	Alpha-1-protease inhibitor	ND	3.37	32.17	D00675
	Alpha-2 antiplasmin	ND	3.38	30.03	AY216659
	Alpha-fibrinogen	5.77	5.05	33.13	M35601
	Brain 4.1(L)	ND	2.24	29.48	AB019257
	CYP1A1	ND	425.81	26.13	K02246
	CYP1B1	ND	3.90	34.60	X83867
	Cathepsin B	ND	2.11	19.33	X82396
	Creatine kinase-B	ND	2.62	29.12	M57664
	Cytosolic NADP-dependent isocitrate dehydrogenase	ND	3.77	24.51	L35317
	Fibrinogen B-beta-chain	5.87	7.95	30.89	M27220
	Glutathione S-transferase Ya subunit	ND	4.27	31.73	M26874
	NADH dehydrogenase (ubiquinone) Fe-S protein 7	ND	2.99	26.11	BC013503
	NC1 protein (nc1 gene)	ND	2.25	28.63	AJ250730
	Peroxisomal enoyl hydratase-like protein (PXEL)	ND	2.01	22.38	U08976
	Protein C	3.91	4.10	29.36	X64336
	Prothrombin precursor (F2 gene)	4.38	5.92	24.44	X52835
	RASP1	ND	2.52	31.93	U55765
	Stearoyl-CoA desaturase 2	ND	2.31	29.98	AB032243
	Tissue factor protein	1.93	2.29	25.09	U07619
Transcription Factor	Zinc finger homeodomain enhancer-binding protein-1 (Zfhep-1)	ND	2.36	32.92	U51583
Immunity Protein	Da1-24	3.17	2.64	—	AY325253
	Interleukin-12 p40 precursor	ND	1.96	35.40	AF133197
	MHC class I antigen (RT1-E gene)	ND	2.42	—	AJ306619
	MHC class I protein	ND	6.46	—	L26224
	Pregnancy-specific glycoprotein (mCGM3)	ND	2.17	—	U09815
Signal Transducer	Beta ig-h3	ND	2.73	31.93	AF305713
	CXC chemokine LIX	ND	2.60	31.90	U90448
	Inhibin alpha-subunit	ND	1.98	27.41	M36453
	Interferon beta	ND	5.07	36.92	D87919
	Interferon inducible protein 10 (IP-10)	5.03	9.48	25.38	U22520
	Macrophage inflammatory protein-2	ND	6.29	32.48	AB060092
	Monokine induced by interferon gamma (Mig)	ND	3.28	33.97	AF537208
	Proliferin-related protein	1.94	1.82	24.23	AF139809
Transporter	Alpha-fetoprotein (AFP)	ND	5.47	27.57	X02361
	ApolipoproteinA-I	ND	6.26	26.66	M00001
	Apolipoprotein A-IV	5.07	4.24	21.71	M00002
	Apolipoprotein B	3.36	7.07	28.26	M27440
	Beta-2 glycoprotein I	5.10	6.28	30.95	X15551
	Beta-globin	ND	3.71	13.83	X16417
	GLUT2	ND	7.39	31.47	J03145
	GLUT4	ND	2.84	31.49	D28561
	Retinol-binding protein (RBP)	2.75	5.39	32.55	M10934
	Transferrin	5.89	4.12	22.82	X77158
	Transferrin-like	ND	4.08	26.01	AF476964
Structural Protein and Other Groups	Angiopoietin-related protein 3	ND	8.90	30.40	*CB581433
	Claudin 2	2.29	3.27	26.96	*BM392116
	Collagen alpha 1 type XI	ND	2.60	33.72	AJ005396
	Collagen type XXVII proalpha 1 chain (col27a1)	ND	1.98	28.20	AY232999

Table 1. (continued)

Molecular function	Description	Array ratio	Real Time PCR ratio	Ct	Accession
	Decorin	ND	2.07	24.20	X59859
	Ficolin-B	ND	2.33	29.23	AB036792
	Glucocorticoid-attenuated response gene 16	ND	92.29	27.14	AJ276893
	Glucocorticoid-attenuated response gene 39	ND	5.54	28.07	*CB719539
	Hypothetical protein RMT-7	ND	2.09	23.13	AF465614
	Interferon-inducible protein homologue	ND	6.15	24.96	*CB610262
	Interferon, alpha-inducible protein (G1p2)	ND	2.76	23.17	*CB790136
	Matrix metalloproteinase inhibitor (TIMP-1)	2.15	2.11	25.20	L31883
	Mx1	4.51	6.41	26.00	X52711
	Mx2	3.80	7.27	25.71	X52712
	Mx3	ND	3.06	26.70	X52713
	Prealbumin	2.04	4.76	27.03	K03252
	Pro alpha 1 collagen type III	ND	2.56	26.78	X70369
	Proteasome subunit R-RING12	ND	2.92	27.78	D10757
	Ribosomal protein L5	ND	2.34	20.59	X06148
	Similar to PC-LKC gene product	1.92	2.06	27.53	*BI291884
	Similar to vinculin	ND	1.99	27.73	*CB757866
	Spp-24 precursor	3.03	6.13	25.56	U19485
	TORID	ND	2.53	25.27	AF370882
	Thrombospondin	ND	2.30	28.72	*AB113080
	Type VI collagen alpha3 subunit	1.92	1.94	25.49	*AI176126
Function Unknown	AB113071	ND	2.37	31.85	*AB113071
	Clone nrhy5-00111-g2	ND	3.17	27.96	*CB546450
	DRNBNB02	ND	2.06	24.98	*BG671212
	EST196998	1.98	2.16	30.78	*AA893195
	LRRGT00077	ND	2.29	30.17	*AY387063
	UI-R-BJ0p-afw-e-10-0-UI.r1	ND	2.14	27.92	*BF566943
	UI-R-C4-akz-c-07-0-UI.s1	3.22	2.99	24.70	*AW531805
	UI-R-E0-bq-f-06-0-UI.r1	ND	5.64	30.34	*BF550478
	Unknown	ND	2.05	26.30	ND

ND: Not determined, Ct: cycle threshold, *: Rat EST database

Two characteristic profiles of the induction were (1) glucose transporters and (2) interferon-related genes, details of which will be described elsewhere.

TCDD-suppressive genes in the placenta

As listed in Table 2, 21 genes were identified as TCDD-suppressive genes in the placenta, 10 genes of which were from the results of the DNA microarray analysis. Six genes were reported only on EST databases, and three genes showed no significant similarity to any gene on existing DNA databases. Other genes were all annotated as shown in Table 2 including those homologues of human or mouse.

Induction of glucose transporter family genes

As shown in Fig. 1, expressions of four major glucose transporter genes were examined. Quantitative real-time PCR revealed that GLUT2 and GLUT4 were strongly induced by the TCDD treatment in the placenta. Gene expression of GLUT3 was also marginally increased by the treatment (1.58-fold), but that of GLUT1 was less affected (1.24-fold). In the control placenta, GLUT3 was abundantly expressed (Ct26.57), while expression levels of the other three transporter genes were relatively low (Ct32.73 for GLUT1, Ct31.47 for GLUT2, and Ct31.49 for GLUT4). Therefore, in addition to the remarkable induction of GLUT2 and GLUT4 genes, a small but significant increase in GLUT3 gene expression may have a major physiolog-

Table 2. TCDD-suppressive genes in the rat placenta

Molecular function	Description	Array ratio	Real Time PCR ratio	Ct	Accession
Enzyme	Urokinase-type plasminogen activator	0.48	0.45	27.99	X63434
	LASP-1	ND	0.19	25.46	AF242187
Signal Transducer	Hepatic product spot 14	0.43	0.33	31.78	K01934
	Prepronociceptin	0.59	0.63	25.84	X97375
	Prolactin-like protein H	0.50	0.41	27.74	AB009889
Transcription Factor	Transcription factor GATA-1	0.55	0.47	31.50	D13518
	Zinc finger protein 52	ND	0.16	34.17	*CK470357
Transporter	mBLVR	ND	0.54	25.50	*CB557112
Structural Protein and Other Groups	Talin	ND	0.35	26.13	*CK366133
Function Unknown	Ab2-225	0.56	0.60	27.78	AY325197
	BB857172	ND	0.16	29.50	*BB857172
	Clone mrpe4-00034-a12	ND	0.16	32.27	*CB760299
	Eker rat-associated intracisternal-A	ND	0.43	32.27	U23776
	EST224029	0.59	0.62	24.96	*AI180286
	FAD104	ND	0.49	25.21	*CB702955
	Nuclear-localized inactive X-specific transcript (Xist)	0.27	0.33	27.18	*AI228978
	UI-R-BJ1-auz-g-11-0-UI.s1	ND	0.31	25.56	*BE111117
	UI-R-CX0s-cct-f-09-0-UI.s1	0.43	0.54	27.16	*BI284907
	Unknown mRNA	0.43	0.48	26.53	AF152002
	Unknown	ND	0.45	31.31	ND
	Unknown	ND	0.51	24.21	ND

ND: Not determined, Ct: Cycle threshold, *: Rat EST database

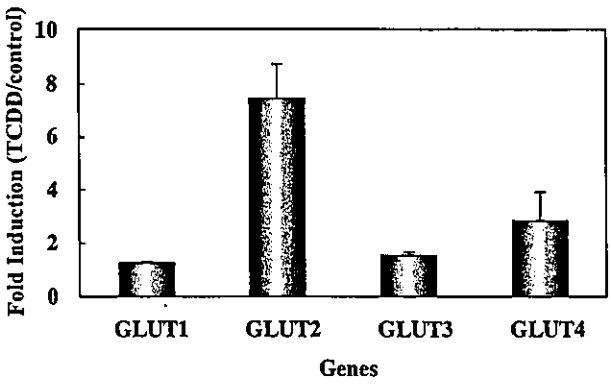

Fig. 1. Induction of glucose transporter genes in the rat placenta by TCDD.
Expression levels of major 4 glucose transporter genes were determined by quantitative real-time PCR, and changes in the expression levels were compared. Values were expressed as fold induction (TCDD/control). Serial dilutions of five points for each sample were used to make each dilution curve. TATA binding protein (TBP) was used as an internal standard to ensure equal loading of template cDNA molecules.

ical significance of the glucose-uptake in the TCDD-treated placenta.

Induction of interferon-related genes

One of the most remarkable findings of the pesent experiment was that many interferon-regulated genes were induced in the placenta of TCDD-treated animals. As shown in Fig. 2, 15 out of 18 interferon-inducible genes examined were strongly up-regulated by the TCDD treatment. Among them were interferon-inducible cytokines, such as IP-10 [17, 18], macrophage inflammatory protein-2, monokine induced by gamma interferon (Mig) [19] and CXC chemokine LIX [20]. Of these, IP-10 was reported to be involved in the interferon-mediated inhibition of angiogenesis [17, 18]. Since many interferon-inducible genes were up-regulated by the TCDD-treatment, we examined the levels of interferon family genes. At the transcription levels, the interferon beta gene was up-regulated (5.07-fold induction) in the TCDD-treated placenta (Table. 1), but we were not able to detect interferon-alpha and -gamma genes in our system (data not shown).

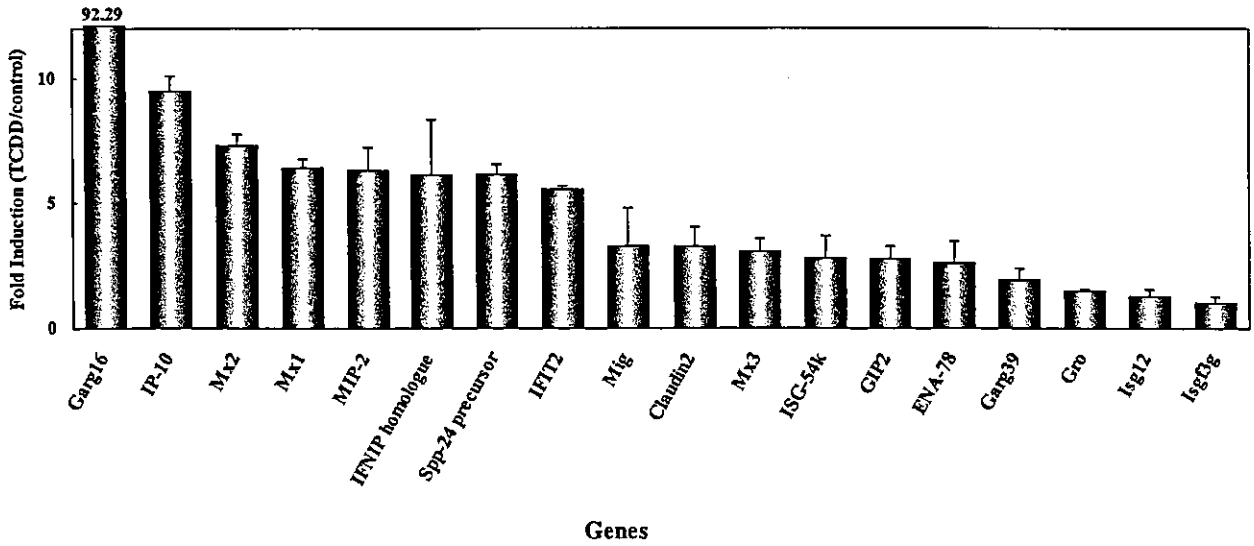

Fig. 2. Induction of interferon regulated genes in the rat placenta by TCDD.
Expression levels of 18 interferon regulated genes were determined by quantitative real-time PCR, and changes in the expression levels were compared. Values were expressed as fold induction (TCDD/control). Serial dilutions of five points for each sample were used to make each dilution curve. TATA binding protein (TBP) was used as an internal standard to ensure equal loading of template cDNA molecules.

Discussion

Previous studies have shown that a very low dose of TCDD results in the increased incidence of fetal death [8, 9]. Histological and protein profiling analysis revealed that the fetal death after the TCDD treatment may be due to the placental hypoxia [9]. In order to evaluate further the mechanisms of the induction of such the adverse effect, comprehensive analysis was done to examine changes in the placental gene expression. As clearly shown in Fig. 1, glucose transporter genes were all induced after the TCDD treatment. Ishimura *et al.* previously reported the histopathological changes in glycogen cells and the elevated levels of glucose content and GLUT3 mRNA expression in the placenta of the TCDD-exposed rats in comparison to those of the control rats [9]. In addition to GLUT3 mRNA, we showed here that GLUT2 and GLUT4 mRNAs were strongly induced by the TCDD-treatment, and that GLUT1 mRNA was less affected by the treatment, indicating that most of major glucose transporter genes were up-regulated by TCDD, which may lead to glycogen accumulation in the placenta. In our quantitative real-time PCR system, values of cycle threshold (Ct) represent expression levels of genes. The Ct value of GLUT3 mRNA was much lower than those of other GLUT family genes, suggesting that the major glucose transporter working in the placenta may be GLUT3, though strong induction of GLUT2 and GLUT4 genes may also play significant roles in the glucose accumulation in the TCDD-treated placenta. As far as we know, this is the first report describing that GLUT2 and GLUT4 genes were actually expressed in the placenta under specific conditions such as the TCDD treatment. It is likely that a tissue-specific responsive mechanism of TCDD exists for the induction of glucose transporters in the placenta, since those transporter genes were not up-regulated in other tissues such as the ovary from the same TCDD-treated animals (data not shown). Histological studies by Ishimura *et al.* showed that blood vessel formation in the placenta was severely impaired by the TCDD treatment (unpublished data), indicating that the angiogenesis was inhibited in the placentas of TCDD-treated animals on GD20. Therefore, the TCDD treatment may cause hypoxic conditions in placenta. It was reported that the expression of GLUT-1 and GLUT-3 mRNAs was up-regulated under hypoxic conditions [21].

Most striking observation of this experiment was that many interferon-inducible genes were up-regulated in the placenta of TCDD-treated animals. As shown in Fig. 2, 15 out of 18 interferon-inducible genes examined were induced by the TCDD treatment, which strongly suggests that interferon signaling pathway

[22] was activated by the TCDD treatment. We also examined the expression levels of interferon-alpha, -beta, and -gamma by the real-time PCR analysis. Only interferon-beta gene expression was detected, and the level was strongly up-regulated by the TCDD treatment. Although the data suggest that interferon-beta is the key factor, we must take into consideration of the fact that the interferon signaling pathway is activated by many other signaling molecules [23]. The typical interferon signaling pathway is activated through the JAK-STAT system [22]. It is well known that pituitary hormone GH and prolactin also activate the JAK-STAT system [23], and that several prolactin-like molecules including placental lactogen are abundantly produced in the placenta [24]. We can not exclude the possibility that, in addition to interferon-beta, the prolactin-like molecules produced in the placenta may also play significant roles in the induction of interferon-regulated genes.

It is noteworthy that interferon is known to be involved in the regulation of angiogenesis. Interferon-alpha and -gamma were reported to inhibit endothelial cell proliferation [25]. IP-10, one of the interferon-inducible genes, was also strongly induced in the TCDD-treated rat placenta. IP-10 is a member of the alpha-chemokine family, inhibits bone marrow colony formation, has anti-tumor activity *in vivo*, is chemoattractant for monocytes and T cells, and promotes T cell adhesion to endothelial cells. In addition to the above functions, IP-10 has been reported to be a potent inhibitor of angiogenesis *in vivo* [17, 18]. Furthermore, thrombospondin [26] and tissue inhibitor of metalloproteinase 1 (TIMP-1) [27] were also induced by the TCDD treatment, both of which are known to inhibit endothelial cell proliferation. Considering the above observations, the neovascularization in the placenta on GD20 may be impaired by the TCDD treatment through the induction of anti-angiogenic factors.

It is reasonable to speculate that the hypoxic state in the placentas of TCDD-treated rats may be due to the impairment of angiogenesis in the placenta, which may be caused by the activation of the interferon signaling pathway including the production of angiogenesis-inhibitory cytokine IP-10 as well as the production of anti-angiogenic factors such as thrombospondin and TIMP-1.

In conclusion, we identified 81 dioxin-inducible genes and 21 dioxin-suppressive genes from the placenta of TCDD-treated Holtzman rats on GD20. The present study revealed that glucose transporters were strongly up-regulated by the TCDD treatment.

In addition, many interferon-inducible genes were also up-regulated by the TCDD treatment, including IP-10, a potent angiogenesis-inhibitory cytokine. Activation of the interferon signaling pathway and the induction of anti-angiogenic factors may result in the hypoxic state of placenta, which may lead to the increased incidence of fetal death.

Acknowledgement

The authors thank Yoshiko Inoue for her assistance in manuscript preparation, and T. Nobe for DNA microarray operations. This work was supported in part by grants from the Smoking Research Foundation, Japan Science and Technology Agency, and the Ministry of Health, Welfare and Labour, by 21st Century COE Program (Medical Science), and by the Program for Promotion of Fundamental Studies in Health Sciences of Pharmaceuticals and Medical Devices Agency (PMDA) of Japan.

References

1. Couture L, Abbott B, Birnbaum L (1990) A critical review of the developmental toxicity and teratogenicity of 2,3,7,8-tetrachlorodibenzo-p-dioxin: recent advances toward understanding the mechanism. *Teratology* 42: 619–627.
2. Birnbaum L (1995) Developmental effects of dioxins and related endocrine disrupting chemicals. *Toxicol Lett* 82–83: 743–750.
3. Lindstrom G, Hooper K, Petreas M, Stephens R, Gilman A (1995) Workshop on perinatal exposure to dioxin-like compounds. I. Summary. *Environ Health Perspect* 103: 135–142.
4. Ohsako S, Miyabara Y, Nishimura N, Kurosawa S, Sakaue M, Ishimura R, Sato M, Takeda K, Aoki Y, Sone H, Tohyama C, Yonemoto J (2001) Maternal exposure to a low dose of 2,3,7,8-tetrachlorodibenzo-p-dioxin (TCDD) suppressed the development of reproductive organs of male rats: dose-dependent increase of mRNA levels of 5alpha-reductase type 2 in contrast to decrease of androgen receptor in the pubertal

ventral prostate. *Toxicol Sci* 60: 132–143.
5. Couture L, Harris M, Birnbaum L (1990) Characterization of the peak period of sensitivity for the induction of hydronephrosis in C57BL/6N mice following exposure to 2,3,7,8-tetrachlorodibenzo-p-dioxin. *Fundam Appl Toxicol* 15: 142–150.
6. Schecter A, Olson J, Papke O (1996) Exposure of laboratory animals to polychlorinated dibenzodioxins and polychlorinated dibenzofurans from commercial rodent chow. *Chemosphere* 32: 501–508.
7. Guo Y, Hendrickx A, Overstreet J, Dieter J, Stewart D, Tarantal A, Laughlin L, Lasley B (1999) Endocrine biomarkers of early fetal loss in cynomolgus macaques (Macaca fascicularis) following exposure to dioxin. *Biol Reprod* 60: 707–713.
8. Ishimura R, Ohsako S, Miyabara Y, Sakaue M, Kawakami T, Aoki Y, Yonemoto J, Tohyama C (2002) Increased glycogen content and glucose transporter 3 mRNA level in the placenta of Holtzman rats after exposure to 2,3,7,8-tetrachlorodibenzo-p-dioxin. *Toxicol Appl Pharmacol* 178: 161–171.
9. Ishimura R, Ohsako S, Kawakami T, Sakaue M, Aoki Y, Tohyama C (2002) Altered protein profile and possible hypoxia in the placenta of 2,3,7,8-tetrachlorodibenzo-p-dioxin-exposed rats. *Toxicol Appl Pharmacol* 185: 197–206.
10. Pastorian K, Hawel L, Byus C (2000) Optimization of cDNA representational difference analysis for the identification of differentially expressed mRNAs. *Anal Biochem* 283: 89–98.
11. Mizutani T, Sonoda Y, Minegishi T, Wakabayashi K, Miyamoto K (1997) Cloning, characterization, and cellular distribution of rat scavenger receptor class B type I (SRBI) in the ovary. *Biochem Biophys Res Commun* 234: 499–505.
12. Sekiguchi T, Mizutani T, Yamada K, Yazawa T, Kawata H, Yoshino M, Kajitani T, Kameda T, Minegishi T, Miyamoto K (2002) Transcriptional regulation of the epiregulin gene in the rat ovary. *Endocrinology* 143: 4718–4729.
13. Mizutani T, Yamada K, Yazawa T, Okada T, Minegishi T, Miyamoto K (2001) Cloning and characterization of gonadotropin-inducible ovarian transcription factors (GIOT1 and -2) that are novel members of the (Cys)(2)-(His)(2)-type zinc finger protein family. *Mol Endocrinol* 15: 1693–1705.
14. Lancaster J, Dressman H, Whitaker R, Havrilesky L, Gray J, Marks J, Nevins J, Berchuck A (2004) Gene expression patterns that characterize advanced stage serous ovarian cancers. *J Soc Gynecol Investig* 11: 51–59.
15. Whitlock JJ (1999) Induction of cytochrome P4501A1. *Annu Rev Pharmacol Toxicol* 39: 103–125.
16. Whitlock JJ, Chichester C, Bedgood R, Okino S, Ko H, Ma Q, Dong L, Li H, Clarke-Katzenberg R (1997) Induction of drug-metabolizing enzymes by dioxin. *Drug Metab Rev* 29: 1107–1127.
17. Angiolillo A, Sgadari C, Taub D, Liao F, Farber J, Maheshwari S, Kleinman H, Reaman G, Tosato G (1995) Human interferon-inducible protein 10 is a potent inhibitor of angiogenesis *in vivo*. *J Exp Med* 182: 155–162.
18. Strieter R, Kunkel S, Arenberg D, Burdick M, Polverini P (1995) Interferon gamma-inducible protein 10 (IP-10), a member of the C-X-C chemokine family, is an inhibitor of angiogenesis. *Biochem Biophys Res Commun* 210: 51–57.
19. Singh U, Singh S, Iqbal N, Weaver C, McGhee J, Lillard JJ (2003) IFN-gamma-inducible chemokines enhance adaptive immunity and colitis. *J Interferon Cytokine Res* 23: 591–600.
20. Neumann B, Emmanuilidis K, Stadler M, Holzmann B (1998) Distinct functions of interferon-gamma for chemokine expression in models of acute lung inflammation. *Immunology* 95: 512–521.
21. Semenza G (1999) Regulation of mammalian O2 homeostasis by hypoxia-inducible factor 1. *Annu Rev Cell Dev Biol* 15: 551–578.
22. Leonard W (2001) Role of Jak kinases and STATs in cytokine signal transduction. *Int J Hematol* 73: 271–277.
23. Yu-Lee L (2002) Prolactin modulation of immune and inflammatory responses. *Recent Prog Horm Res* 57: 435–455.
24. Southard J, Talamantes F (1991) Placental prolactin-like proteins in rodents: variations on a structural theme. *Mol Cell Endocrinol* 79: 133–140.
25. Friesel R, Komoriya A, Maciag T (1987) Inhibition of endothelial cell proliferation by gamma-interferon. *J Cell Biol* 104: 689–696.
26. Good D, Polverini P, Rastinejad F, Le Beau M, Lemons R, Frazier W, Bouck N (1990) A tumor suppressor-dependent inhibitor of angiogenesis is immunologically and functionally indistinguishable from a fragment of thrombospondin. *Proc Natl Acad Sci USA* 87: 6624–6628.
27. Takigawa M, Nishida Y, Suzuki F, Kishi J, Yamashita K, Hayakawa T (1990) Induction of angiogenesis in chick yolk-sac membrane by polyamines and its inhibition by tissue inhibitors of metalloproteinases (TIMP and TIMP-2). *Biochem Biophys Res Commun* 171: 1264–1271.

MOLECULAR AND CELLULAR BIOLOGY, Jan. 2005, p. 136–146 Vol. 25, No. 1
0270-7306/05/$08.00+0 doi:10.1128/MCB.25.1.136–146.2005

Cyclic AMP Potentiates Vascular Endothelial Cadherin-Mediated Cell-Cell Contact To Enhance Endothelial Barrier Function through an Epac-Rap1 Signaling Pathway

Shigetomo Fukuhara,[1] Atsuko Sakurai,[1] Hideto Sano,[2] Akiko Yamagishi,[1] Satoshi Somekawa,[1,3] Nobuyuki Takakura,[2] Yoshihiko Saito,[3] Kenji Kangawa,[4] and Naoki Mochizuki[1]*

Department of Structural Analysis[1] and Department of Biochemistry,[4] National Cardiovascular Center Research Institute, Osaka, Department of Stem Cell Biology, Cancer Research Institute, Kanazawa University, Kanazawa,[2] and First Department of Internal Medicine, Nara Medical University, Nara,[3] Japan

Received 2 August 2004/Returned for modification 2 September 2004/Accepted 28 September 2004

Cyclic AMP (cAMP) is a well-known intracellular signaling molecule improving barrier function in vascular endothelial cells. Here, we delineate a novel cAMP-triggered signal that regulates the barrier function. We found that cAMP-elevating reagents, prostacyclin and forskolin, decreased cell permeability and enhanced vascular endothelial (VE) cadherin-dependent cell adhesion. Although the decreased permeability and the increased VE-cadherin-mediated adhesion by prostacyclin and forskolin were insensitive to a specific inhibitor for cAMP-dependent protein kinase, these effects were mimicked by 8-(4-chlorophenylthio)-2′-*O*-methyladenosine-3′, 5′-cyclic monophosphate, a specific activator for Epac, which is a novel cAMP-dependent guanine nucleotide exchange factor for Rap1. Thus, we investigated the effect of Rap1 on permeability and the VE-cadherin-mediated cell adhesion by expressing either constitutive active Rap1 or Rap1GAPII. Activation of Rap1 resulted in a decrease in permeability and enhancement of VE-cadherin-dependent cell adhesion, whereas inactivation of Rap1 had the counter effect. Furthermore, prostacyclin and forskolin induced cortical actin rearrangement in a Rap1-dependent manner. In conclusion, cAMP-Epac-Rap1 signaling promotes decreased cell permeability by enhancing VE-cadherin-mediated adhesion lined by the rearranged cortical actin.

Endothelial cells lining blood vessels regulate endothelial barrier function, which restricts the passage of plasma proteins and circulating cells across the endothelial cells. Endothelial barrier dysfunction results in an increase in vascular permeability, thereby causing edema or inflammatory or metastatic cell infiltration. Inflammatory mediators such as thrombin and histamine induce intercellular gap formation, leading to an increase in endothelial permeability (1, 4). In contrast, angiopoietin 1 and sphingosine-1-phosphate (S1P) stabilize endothelial barrier integrity (17, 18). In addition, cyclic AMP (cAMP), a second messenger downstream of Gs-coupled receptor, improves endothelial cell barrier function (32, 39, 43). Consistently, cAMP-elevating G protein-coupled receptor (GPCR) agonists, adrenomedullin (AM), prostacyclin (PGI2), prostaglandin E2 (PGE2), and β-adrenergic agonists reduce endothelial hyperpermeability induced by inflammatory stimuli (15, 19, 25).

The endothelial cell barrier is structurally organized by adherens junctions (AJ) and tight junctions. Vascular endothelial (VE) cells express both VE-cadherin (also known as cadherin-5 and CD144) and neural (N)-cadherin (9, 33). VE-cadherin constitutes AJ, whereas N-cadherin formed the cell-cell contacts between endothelial cells and endothelial cell-supporting pericytes. VE-cadherin mediates calcium-dependent, homophilic intercellular adhesion. Its short cytoplasmic tail binds to three armadillo family proteins, β-, γ-, and p120-catenins. β- and γ-catenins associated with α-catenin link the VE-cadherin complex to the actin cytoskeleton and, therefore, strengthen the AJ adhesiveness (9).

Endothelial AJ are dynamic structures, and their adhesive property is finely regulated by several different mechanisms. Tyrosine phosphorylation of VE-cadherin, β-catenin, and p120-catenin correlates with weakened endothelial cell-cell adhesion. VE growth factors and inflammatory mediators such as histamine and thrombin induce tyrosine phosphorylation of AJ components, resulting in the weakened cell-cell contacts and increased endothelial cell permeability (1, 14, 40). In clear contrast, angiopoietin 1, which stabilizes cell-cell contacts, induces dephosphorylation of endothelial cell adhesion molecules, VE-cadherin, and platelet endothelial cell adhesion molecule 1 (17). It has been also reported that S1P induces AJ formation and enhances barrier function through a Rac-dependent cortical actin rearrangement (18). cAMP-dependent protein kinase A (PKA) is suggested to be crucial for cAMP-triggered stabilization of cell-cell contacts and for barrier integrity of endothelial cells (43). However, it has not been clear whether PKA-independent signaling is involved in the regulation of endothelial barrier function.

Rap1, belonging to Ras family GTPase, is involved in the formation and stabilization of AJ in *Drosophila melanogaster* (23). Rap1 becomes the GTP-bound active form by guanine

* Corresponding author. Mailing address: Department of Structural Analysis, National Cardiovascular Center Research Institute, 5-7-1 Fujishirodai, Suita, Osaka 565-8565, Japan. Phone: 81-6-6833-5012, ext. 2508. Fax: 81-6-6835-5461. E-mail: nmochizu@ri.ncvc.go.jp.

nucleotide exchange factor (GEF) and the GDP-bound inactive form by GTPase-activating proteins (GAP), respectively. GEFs for Rap1 include C3G, CalDAG-GEFs, Epacs, and DOCK4 (reviewed in reference 6). DOCK4, which is disrupted in various types of human cancers, regulates the formation of AJ (41). Very recent reports also revealed that Rap1 activity is required for the formation of E-cadherin-based cell-cell contacts (20, 36). These findings prompted us to investigate how Rap1 is activated to stabilize cell-cell contacts and to examine the physiological consequence of stabilized cell-cell contacts by Rap1.

In the present study, we investigated the mechanism by which cAMP-elevating GPCR agonists potentiate endothelial barrier function and restrict cell permeability. We found that increased cAMP triggers Epac-Rap1 signaling to reduce permeability independently of PKA by augmentation of VE-cadherin-mediated cell-cell adhesion.

MATERIALS AND METHODS

Reagents and antibodies. Human recombinant AM was kindly provided by Shionogi & Co. Ltd (31). Materials were purchased as follows: isoproterenol (Iso), PGE2, PGI2, thrombin, forskolin (FSK), and 3-isobutyl-1-methylxanthine (IBMX) from Wako Pure Chemical Industries; dibutyryl-cAMP (dbcAMP) from Sigma-Aldrich; H89 from Seikagaku Corporation; 8-(4-chlorophenylthio)-2′-*O*-methyladenosine-3′,5′-cyclic monophosphate (8-CPT-2′-O-Me-cAMP) from Tocris; fluorescein isothiocyanate (FITC)-labeled dextran (molecular weight, 42,000) and purified human immunoglobulin G (IgG) Fc protein from ICN Biologicals; vascular endothelial growth factor (VEGF) from R & D Systems. Anti-Rap1GAPII antibody was developed by immunization of glutathione *S*-transferase (GST)-tagged Rap1GAPII (amino acids 411 to 694 of Rap1GAPII). Other antibodies used here were purchased as follows: anti-VE-cadherin from Chemicon International and Transduction Laboratories; anti-β-catenin from Transduction Laboratories; anti-CREB and anti-phospho-CREB (Ser133) from Cell Signaling Technology; anti-Rap1 from Santa Cruz Biotechnology; anti-cortactin from Upstate Biotechnology, Inc.; rhodamine-phalloidin and Alexa 488-labeled goat anti-mouse IgG from Molecular Probes; horseradish peroxidase-coupled goat anti-mouse and goat anti-rabbit IgG from Amersham Biosciences.

Cell culture and transfection. Human umbilical vein endothelial cells (HUVECs) and human arterial endothelial cells (HAECs) were purchased from Kurabo (Kurashiki, Japan). The cells were maintained in HuMedia-EG2 with a growth additive set as described previously (12) and used for experiments before passages 7 and 10, respectively. HEK293, 293T, and HeLa cells were maintained in Dulbecco's modified Eagle's medium (DMEM; Nissui, Tokyo, Japan) supplemented with 10% fetal bovine serum and antibiotics (100 μg of streptomycin/ml and 100 U of penicillin/ml). HUVECs and 293T cells were transfected by using Lipofectamine Plus reagent (Invitrogen) and by the calcium-phosphate precipitation technique, respectively.

Plasmids and adenovirus. pcDNA-VE-cad-Ect-Fc-His is a modified vector of pcDNA3.1-Fc-PECAM-1 (a kind gift from W. A. Muller, Cornell University) for producing the secreted form of the extracellular domain of VE-cadherin fused with Fc followed by a six-His tag. A DNA fragment encoding human Epac lacking the cAMP binding domain (amino acids 324 to 881) was amplified by PCR with pMT2SM-HA-Epac (a kind gift from J. L. Bos, Utrecht University, Utrecht, The Netherlands) as a template and ligated into the pCXN2 vector (12). pCXN2-FLAG-Rap1V12-IRES-EGFP expressed both FLAG-tagged Rap1V12 and internal ribosomal entry site (IRES)-driven enhanced green fluorescent protein (EGFP), and pCXN2-Rap1GAPII-IRES-EGFP expressed both FLAG-tagged Rap1GAPII and IRES-driven EGFP. pGL3 control vector was purchased from Promega Corp. Recombinant adenoviruses encoding Rap1GAPII (Ad-RapGAP) and LacZ (Ad-LacZ) were obtained from S. Hattori (The Institute of Medical Science, University of Tokyo) and M. Matsuda (Research Institute for Microbial Disease, Osaka University, Osaka, Japan), respectively. Adenoviruses expressing FLAG-tagged Rap1V12 and IRES-driven EGFP (Ad-Flag-Rap1V12-IRES-EGFP) were produced by using the Adeno-X system according to the manufacturer's protocol (Clontech). Endothelial cells were infected with adenoviruses at the appropriate multiplicities of infection (MOI) as described in the figure legends.

Permeability assay. Permeability across the endothelial cell monolayer was measured by using type I collagen-coated transwell units (6.5-mm diameter, 3.0-μm-pore-size polycarbonate filter; Corning Costar Corporation). HUVECs plated at 10^5 cells in each well were cultured for 3 to 4 days before experiments. After serum starvation in medium 199 containing 1% bovine serum albumin (BSA) for 1 h, the cells were treated with the agonists or drugs, as indicated in the figure legends, for 30 min. Permeability was measured by adding 1 mg of FITC-labeled dextran (molecular weight, 42,000)/ml together with or without 2 U of thrombin/ml to the upper chamber. After incubation for 30 min, 50 μl of sample from the lower compartment was diluted with 300 μl of phosphate-buffered saline (PBS) and measured for fluorescence at 520 nm when excited at 492 nm with a spectrophotometer F-4500 (Hitachi). HUVECs infected with adenovirus for 24 h after becoming confluent and kept for another 24 h in replaced medium were subjected to a cell permeability assay.

Immunocytochemistry. Monolayer-cultured HUVECs grown on a 35-mm-diameter glass base dish (Asahi Techno Glass) were starved in medium 199 containing 0.5% BSA for 3 h and subsequently incubated with the stimulants indicated in the figure legends for 30 min. After stimulation, the cells were fixed in PBS containing 2% formaldehyde for 30 min at 4°C, washed with PBS, and permeabilized with 0.05% Triton X-100 for 30 min at 4°C. Cells were blocked with PBS containing 4% BSA for 1 h at room temperature (RT) and stained with rhodamine-phalloidin for 20 min, anti-VE-cadherin for 60 min, and anticortactin for 60 min at RT. Protein reacting with antibody was visualized with Alexa 488-labeled goat anti-mouse IgG. Images were recorded with a confocal microscope (BX50WI, Fluoview; Olympus) with a water immersion objective lens (LUMPlanF1 100X1.00W).

VE-cadherin translocation assay and Western blot analysis. HUVECs plated in six-well plates were serum starved in medium 199 containing 1% BSA overnight. The cells were stimulated with PGI2 and FSK for the indicated time and fractionated with cytoskeleton-stabilizing buffer (10 mM HEPES [pH 7.4], 250 mM sucrose, 150 mM KCl, 1 mM EGTA, 3 mM $MgCl_2$, 1× protease inhibitor cocktail [Roche Diagnostics], 1 mM Na_3VO_4, 0.5% Triton X-100) by centrifugation at 15,000 × *g* for 15 min. The Triton X-100-insoluble fraction was subjected to sodium dodecyl sulfate-polyacrylamide gel electrophoresis (SDS-PAGE) followed by transfer to Immobilon-P (Amersham Biosciences) and immunoblotting with the indicated antibodies. Immunocomplexes were visualized by enhanced chemiluminescence detection (Amersham Biosciences) with species-matched peroxidase-conjugated secondary antibodies.

Purification of recombinant VE-cadherin ectodomain-Fc chimeric protein. 293T cells transfected with pcDNA-VE-cad-Ect-Fc-His were cultured in DMEM supplemented with 10% fetal calf serum for 24 h and subsequently kept in replaced medium (DMEM-F21 containing 1% fetal calf serum) for 7 days. VE-cadherin-Fc (VEC-Fc) protein secreted into the medium was collected every 2 days and centrifuged to remove floating cells and debris. VEC-Fc was collected on ProBond resin (Invitrogen) by gentle agitation overnight at 4°C. VEC-Fc protein bound to the beads was eluted with 500 mM imidazole, concentrated with Amicon Centriplus 30 (Millipore), and buffer exchanged into PBS containing 2 mM $CaCl_2$ and 2 mM $MgCl_2$ (PBS-Ca/Mg) by dialysis.

Cell adhesion assay. Twenty-four-well tissue culture plates were coated with 10 μg of VEC-Fc or Fc protein/ml in PBS-Ca/Mg at 4°C overnight. After washing with PBS-Ca/Mg, the plates were blocked with 1% heat-inactivated BSA in PBS (heat inactivated at 85°C for 12 min) for 1 h at RT. To examine cell adhesion to the VEC-Fc- or Fc-coated dish, cells were suspended in 0.5% BSA-containing medium 199 and incubated for 30 min at 37°C. Cells (1.5×10^5) were plated on each VEC-Fc- or Fc-coated well in the presence or absence of agonists, drugs, and 5 mM EGTA and adhered to the dish at 37°C for the indicated time. To analyze cell adhesion to a collagen-covered surface, cells were plated onto a collagen-coated six-well plate (Iwaki) and adhered to the dish in the presence or absence of 5 mM EGTA. After washing with PBS-Ca/Mg four times to remove nonadherent cells, adherent cells and input cells were quantified by measuring endogenous alkaline phosphatase activity as described elsewhere (35). Briefly, the cells were lysed in a buffer containing 100 mM Tris-citrate (pH 6.5) and 0.25% Triton X-100, and alkaline phosphate activity in the lysate was measured by using the AttoPhos AP fluorescent substrate system (Promega Corp.). To examine the effects of Rap1V12, EpacΔcAMP, and Rap1GAPII, HUVECs were transfected with plasmids encoding either Rap1V12, EpacΔcAMP, or Rap1GAPII together with the luciferase reporter construct (pGL3 control vector). The adhesion of cells expressing Rap1V12, EpacΔcAMP, or Rap1GAPII to the VEC-Fc-coated dish was normalized by measuring the luciferase activity of the cells and input cells (16).

Detection of GTP-bound form of Rap1. Rap1 activity was assessed by a modified Bos's method as described previously (34). Briefly, HUVECs starved in medium 199 containing 1% BSA overnight were stimulated with the indicated

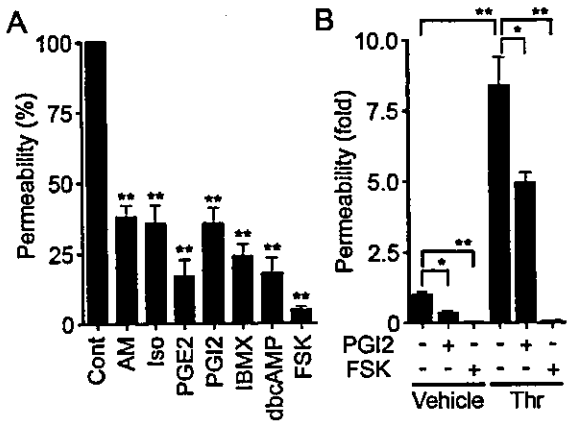

FIG. 1. cAMP enhances barrier function of monolayer VE cells. (A) Vascular permeability, reflecting barrier function, was analyzed by measuring the fluorescence of FITC-labeled dextran across the monolayer-cultured HUVECs as described in Materials and Methods. HUVECs grown on transwell filters were incubated with control (Cont), 0.1 μM AM, 200 μM Iso, 200-ng/ml PGE2, 10-μg/ml PGI2, 1 mM IBMX, 1 mM dbcAMP, and 10 μM FSK for 30 min. Average permeability ± standard deviation is expressed as a percentage compared to the control. (B) The effects of PGI2 and FSK on vascular permeability were quantified in the presence (+) or absence (−) (Vehicle) of 2 U of thrombin (Thr)/ml. Average permeability ± standard deviation is expressed as the increase relative to that observed in unstimulated HUVECs in the vehicle. Data shown are the results from at least three independent experiments. Significant differences from the control (A) or between two groups (B) determined by Student's *t* test are indicated by a single asterisk ($P < 0.05$) or double asterisks ($P < 0.01$).

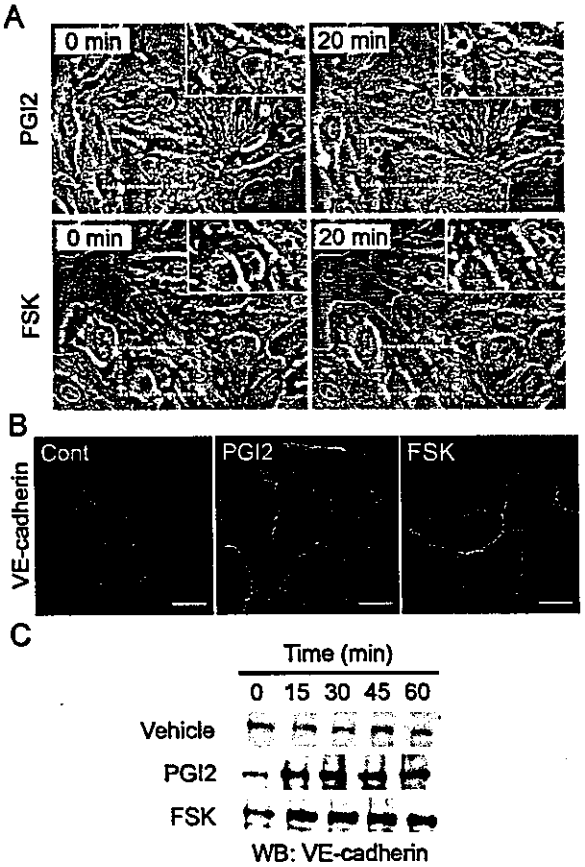

FIG. 2. cAMP induces AJ formation. (A) HUVECs cultured on a glass base dish were stimulated with 10 μg of PGI2/ml (upper panels) or with 10 μM FSK (lower panels) for 20 min and shown as phase-contrast images. Left and right panels show the cells before and after stimulation, respectively. The arrows indicate the sites of cell-cell contacts induced by PGI2 and FSK. The area boxed by the white broken line is enlarged in the right top of the panels. Bars, 50 μm. (B) Subconfluent HUVECs stimulated with vehicle (Cont), 10-μg/ml PGI2, and 10 μM FSK for 45 min were fixed, stained with anti-VE-cadherin antibody, and visualized with Alexa 488-conjugated secondary antibody through a confocal microscope (BX50WI; Olympus). Note that VE-cadherin (green) was accumulated at the cell-cell contact upon PGI2 and FSK stimulation. Bars, 50 μm. (C) Translocation of VE-cadherin was assessed by Triton X-100 solubility. HUVECs were stimulated with vehicle (top), 10-μg/ml PGI2 (middle), and 10 μM FSK (bottom) for the time indicated at the top and fractionated with cytoskeleton-stabilizing buffer as described in Materials and Methods. The Triton X-100-insoluble fraction was subjected to SDS-PAGE followed by Western blot analysis (WB) with anti-VE-cadherin.

agonists and drugs and lysed at 4°C in a pull-down lysis buffer (20 mM Tris-HCl [pH 7.5], 100 mM NaCl, 10 mM $MgCl_2$, 1% Triton X-100, 1 mM EGTA, 1 mM dithiothreitol, 1 mM Na_3VO_4, 1× protease inhibitor cocktail). GTP-bound Rap1 was collected on the GST-Rap1 binding domain of RalGDS precoupled to glutathione-Sepharose beads and subjected to SDS-PAGE followed by immunoblotting with anti-Rap1.

In vivo permeability assay. In vivo permeability was quantified by a modified Miles assay as described previously (29). In brief, ICR mice (Japan SLC, Inc.) shaved 3 days before experiments were lightly anesthetized and intravenously injected with 150 μl of 1% Evans blue dye solution (in saline) passed through a 0.22-μm-pore-size filter. Fifteen minutes later, 20 μl of PBS, VEGF (50 μg/ml), and/or 8-CPT-2′-O-Me-cAMP (1 mM) were applied by intradermal injections with a 30-gauge needle. The sites of intradermal injection were photographed 60 min after the injection, carefully dissected, and weighed. To quantify the vascular permeability, extravasated blue dye was eluted from the dissected skin with formamide at 56°C, and optical density was measured by spectrophotometry at 620 nm.

RESULTS

cAMP enhances the barrier property of monolayer-cultured endothelial cell. To evaluate the barrier function, we examined the permeability of FITC-labeled dextran across monolayer HUVECs. Expectedly, AM, Iso, PGE2, and PGI2 reduced basal endothelial permeability in HUVECs (Fig. 1A). PGI2 also reduced thrombin-induced vascular permeability (Fig. 1B). Other cAMP-elevating bio-ligands similarly reduced thrombin-induced permeability (data not shown). The bio-ligands for cAMP-elevating GPCR that we used in this study indeed increased cAMP in HUVECs (data not shown). Furthermore, IBMX (an inhibitor for phosphodiesterase), dbcAMP (a membrane-permeable cAMP analogue), and FSK (an adenylyl cyclase activator) resulted in a reduction of both basal and thrombin-induced endothelial permeability (Fig. 1; data not shown).

cAMP potentiates formation of AJ. Endothelial barrier function is largely dependent upon endothelial cell junctions. To investigate how cAMP affects AJ formation, we examined AJ organization by immunostaining with anti-VE-cadherin before and after stimulation. When subconfluent HUVECs with intercellular gaps were stimulated with PGI2 or FSK, the cells extended the plasma membrane and established cell-cell contacts with neighboring cells (Fig. 2A). Similar results were

obtained with AM and PGE2 (data not shown). Stimulation of HUVECs with PGI2 and FSK dramatically enhanced accumulation of VE-cadherin at cell-cell contacts (Fig. 2B).

The maturation of AJ requires homophilic binding of intercellular VE-cadherins and tight anchoring to the actin cytoskeleton via the cytoplasmic region through catenins. VE-cadherin anchored to the actin cytoskeleton is detected in detergent-insoluble fractions of cell lysates (26). We found an increase in VE-cadherin in the Triton X-100-insoluble fraction after stimulation with PGI2 or FSK (Fig. 2C). These results suggest that cAMP-elevating GPCR agonists potentiate AJ formation, which results in a cAMP-induced decrease in permeability.

cAMP promotes VE-cadherin-dependent endothelial cell adhesion. VE-cadherin is required for AJ formation (9). To test the involvement of a homophilic interaction of VE-cadherin in cAMP-enhanced AJ formation, we directly examined VE-cadherin-mediated cell adhesion. To mimic the VE-cadherin-dependent cell adhesion, we used VEC-Fc chimeric protein, which consisted of the extracellular domain of VE-cadherin fused to the Fc portion of immunoglobulin. HUVECs were plated onto VEC-Fc-coated dishes and time-lapse imaged. Cells attached within 5 min to the VEC-Fc-coated dish, subsequently spread, and exhibited a typical fried-egg morphology characterized by a large circular lamellipodium (Fig. 3A). No cells attached to the Fc-coated dish (Fig. 3B and C). Since cadherin-dependent cell adhesion requires Ca^{2+}, we examined the effect of Ca^{2+} chelation on cell adhesion to VEC-Fc-coated dishes. Cell adhesion to VEC-Fc-coated dishes was completely abolished by chelating extracellular Ca^{2+}, although cell attachment to the collagen-coated dish was unaffected (Fig. 3C and D). Basal and FSK-augmented cell adhesion to VEC-Fc-coated dishes was inhibited by EGTA (Fig. 3C). Both HUVECs and HAECs expressing VE-cadherin adhered to the VEC-Fc-coated dish (Fig. 3E). In clear contrast, HeLa and HEK293 cells, which express N-cadherin, but not VE-cadherin (20, 42), did not adhere to the VEC-Fc-coated dish, although these cells could attach to the collagen-coated dish (Fig. 3E; data not shown). Collectively, these results indicate that endothelial cell adhesion to the VEC-Fc-coated dish depends upon the homophilic ligation of VE-cadherin.

We proceeded to investigate the effect of cAMP-elevating GPCR agonists on VE-cadherin-mediated cell adhesion. The adhesion of HUVECs plated in the presence of PGI2 or FSK was evaluated by the alkaline phosphatase activity of remaining cells after washing. PGI2 enhanced adhesion of HUVECs to the VEC-Fc-coated dish in a concentration-dependent manner (Fig. 4A) and in a time-dependent manner (Fig. 4B). In a time course analysis, we noticed that enhanced adhesion was observed 7 min after the plating (Fig. 4B). Other cAMP-elevating GPCR agonists, including AM, Iso, and PGE2, potentiated VE-cadherin-dependent cell adhesion (Fig. 4C). In addition, similarly enhanced cell adhesion to the VEC-Fc-coated dish was also observed in the cells treated with cAMP-elevating drugs such as IBMX, dbcAMP, and FSK (Fig. 4F). Like PGI2, the effect of FSK on cell adhesion to the VEC-Fc-coated dish was concentration dependent and time dependent (Fig. 4D and E). This cAMP-induced cell adhesion to the VEC-Fc-coated dish depends on the enhanced homophilic ligation of VE-cadherin because FSK did not augment endothelial adhe-

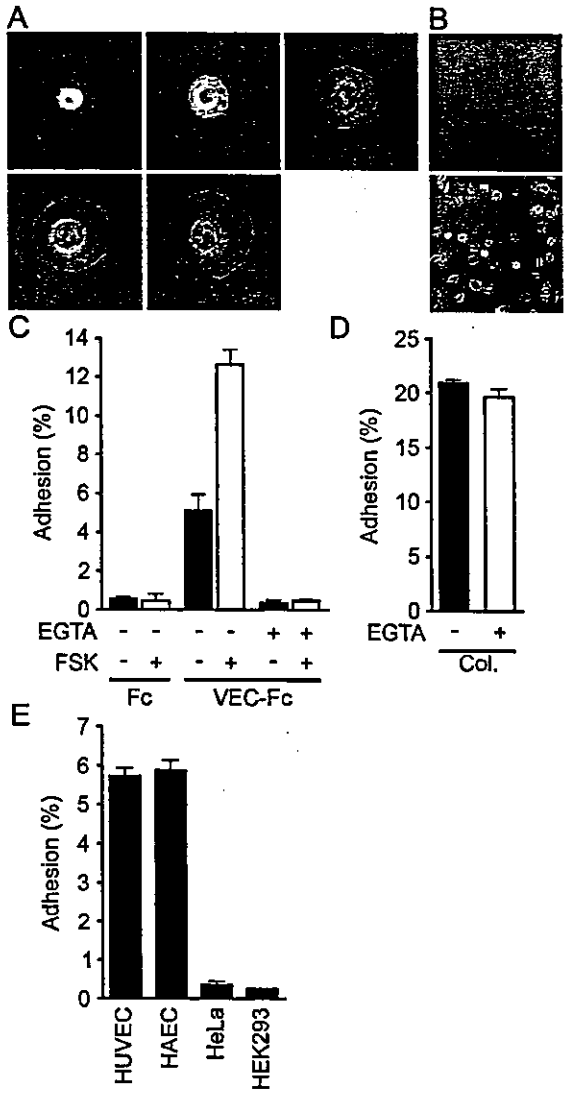

FIG. 3. Endothelial cells adhere to a VEC-Fc-coated dish through homophilic ligation of VE-cadherin. (A) HUVECs were plated onto the VEC-Fc-coated dish and time-lapse imaged at the time points (in minutes) indicated on the panels. Bar, 20 μM. (B) HUVECs were plated on the Fc-coated dish (top panel) or the VEC-Fc-coated dish (bottom panel) for 1 h and phase-contrast imaged after removal of nonadherent cells by washing with PBS-Ca/Mg. (C) HUVECs were plated onto either an Fc- or VEC-Fc-coated dish in the absence (−) or presence (+) of 5 mM EGTA and 10 μM FSK for 7 min. Cell adhesion was quantified as described in Materials and Methods. (D) Adhesion of HUVECs to a collagen-coated dish in the presence or absence of 5 mM EGTA was analyzed by a method similar to that described for panel C. (E) Adhesion of HUVECs, HAECs, and HeLa and HEK293 cells to the VEC-Fc-coated dish was examined as described in the legend for panel C. Cells adhering to the dishes of total input cells (percentage) is expressed as the mean ± standard deviation by measuring alkaline phosphatase activity of adherent cells divided by that of total input cells. Representative results from three independent experiments were shown in all panels.

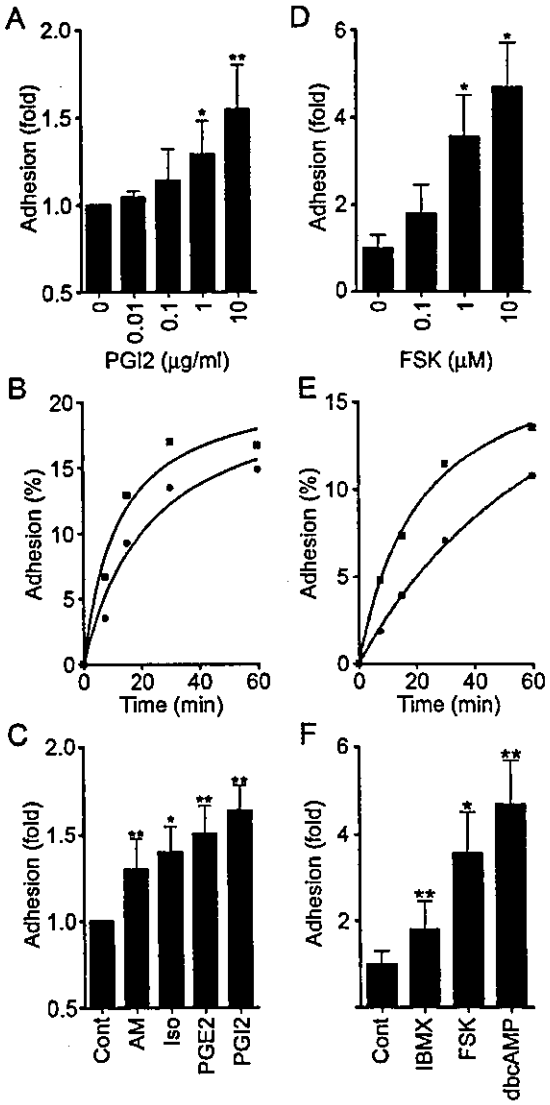

FIG. 4. cAMP potentiates VE-cadherin-dependent cell adhesion. (A) HUVECs were plated onto a VEC-Fc-coated dish in the presence of PGI2 at the concentrations indicated at the bottom for 7 min. Cell adhesion was quantified as described in Materials and Methods. Mean adhesion activity ± standard deviation is expressed as the increase compared with that observed in unstimulated cells. (B) HUVECs were plated onto the VEC-Fc-coated dish in the absence (circle) or presence (square) of 10-μg/ml PGI2 for the time indicated at the bottom. The percent adhesion was calculated by measuring the alkaline phosphatase activity of adherent cells divided by that of total input cells. (C) HUVECs stimulated with cAMP-elevating ligands similar to that described in the legend to panel A were assessed for adhesion activity. The concentration of stimulants was the same as described in the legend to Fig. 1A. (D) The effect of FSK on cell adhesion was analyzed by a method similar to that described for panel A, except that cells were preincubated for 10 min before plating. (E) The effect of 10 μM FSK on time-dependent adhesion was analyzed as described in the legend to panel B, except that cells were preincubated for 10 min before plating. (F) HUVECs stimulated with the reagent indicated at the same concentration used as described in the legend to Fig. 1A were analyzed for cell adhesion by a method similar to that described for panel D. Data are expressed as means ± standard deviations of the results from three independent experiments in panels A, C, D, and F. Representative results from three independent experiments were shown in panels B and E. A significant difference from the control determined by Student's *t* test is indicated with a single asterisk ($P < 0.05$) or double asterisks ($P < 0.01$).

sion to the Fc-coated dish or attachment to the VEC-Fc-coated dish in the absence of extracellular Ca^{2+} (Fig. 3C). These results indicate that cAMP potentiates VE-cadherin-dependent cell adhesion.

cAMP augments endothelial barrier function in a PKA-independent manner. PKA is suggested to be involved in cAMP-enhanced endothelial barrier function (43). Thus, we investigated the involvement of PKA in the regulation of endothelial barrier integrity by PGI2 and FSK. Unexpectedly, PGI2- and FSK-induced reduction of endothelial permeability was insensitive to a specific PKA inhibitor, H89 (7) (Fig. 5A and B). The reduction of thrombin-increased permeability by FSK was also unaffected by H89 (Fig. 5C). Consistently, H89 did not affect VE-cadherin-mediated cell adhesion enhancement by PGI2 and FSK (Fig. 5D and E). To confirm that H89 worked in HUVECs, we examined FSK-induced phosphorylation of CREB, a direct PKA substrate (38). Phosphorylation of CREB upon FSK stimulation was significantly inhibited by H89, indicating the effectiveness of this inhibitor in HUVECs (Fig. 5F). Therefore, these results apparently suggest a novel PKA-independent signaling pathway involved in cAMP-induced endothelial barrier function.

cAMP induces Rap1 activation. Besides PKA, Epac (cAMP-GEF) was identified as a novel cAMP target and a Rap1-specific GEF (5, 21). We therefore hypothesized that cAMP-activated Epac-Rap1 signaling is involved in the enhancement of VE-cadherin-dependent cell adhesion and endothelial barrier function. To address this possibility, we tested whether cAMP-elevating GPCR agonists induce Rap1 activation in HUVECs. Rap1 activity was determined by a pull-down assay by using a GST fusion protein of Rap1-binding domain of RalGDS according to the Bos's method. Bio-ligands for cAMP-elevating GPCR activated Rap1 (Fig. 6A). PGI2 rapidly induced Rap1 activation, which peaked at 1 to 5 min after the stimulation and then declined to the basal level by 10 min (Fig. 6C). A second wave of Rap1 activation was also observed 15 to 45 min after the stimulation (Fig. 6C). PGI2-induced Rap1 activation occurred in a concentration-dependent manner (Fig. 6B), which was associated with enhancement of VE-cadherin-dependent cell adhesion (Fig. 4A). Similarly, dbcAMP, FSK, and IBMX activated Rap1 (Fig. 6D). FSK-induced Rap1 activation reached a maximal level 2 to 5 min after the stimulation, and the level was sustained for up to 15 to 30 min (Fig. 6E). Collectively, these findings indicate that cAMP induces Rap1 activation in endothelial cells.

Specific activation of Epac reduces endothelial permeability and enhances VE-cadherin-dependent cell adhesion. To test whether the activation of endogenous Epac is sufficient to reduce endothelial permeability and to induce VE-cadherin-dependent cell adhesion, we used a recently developed cAMP analog, 8-CPT-2'-O-Me-cAMP, which specifically activates Epac without affecting PKA activity (13). As expected, 8-CPT-2'-O-Me-cAMP induced Rap1 activation in HUVECs (Fig. 7A), indicating that Epac is expressed in endothelial cells.

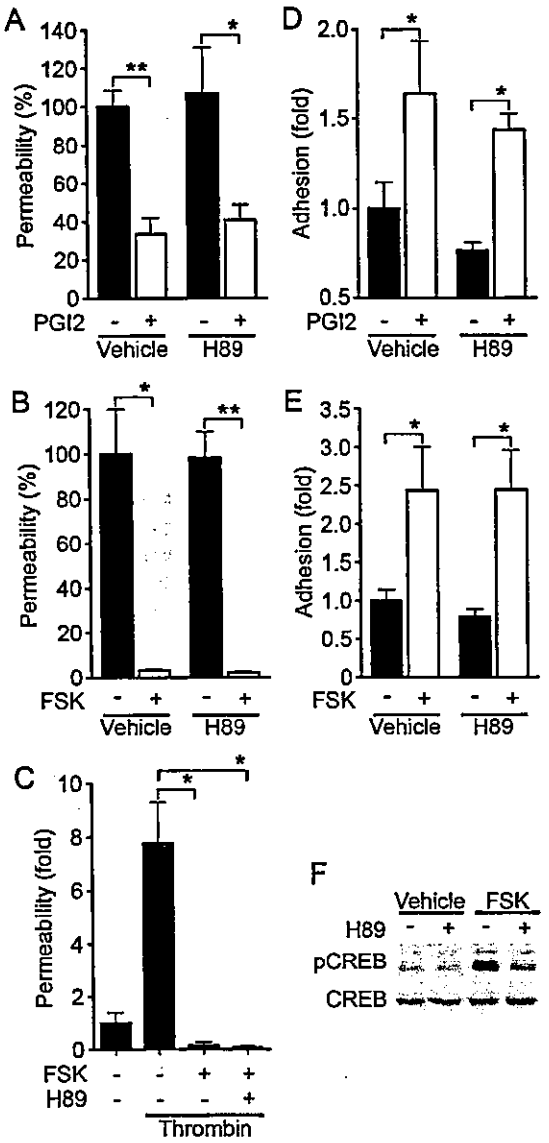

FIG. 5. cAMP-enhanced VE-cadherin-dependent cell adhesion and endothelial barrier function does not depend upon PKA. (A) Permeability across monolayer HUVECs grown on transwell filters were assessed by measuring FITC-labeled dextran as described in the legend to Fig. 1A. The effect of 10-μg/ml PGI2 on cell permeability without pretreatment (Vehicle) or with pretreatment with 5 μM H89, a specific PKA inhibitor, for 10 min is indicated as the percent permeability compared to that observed in untreated cells. +, present; −, absent. (B) The effect of 10 μM FSK on cell permeability without pretreatment (Vehicle) and with pretreatment with H89 was assessed similar to that described for panel A. (C) The effect of pretreatment of HUVECs with 5 μM H89 on FSK-induced reduction of 2-U/ml thrombin-induced permeability was analyzed. Permeability indicates the increase relative to that observed in untreated cells. (D) HUVECs untreated or pretreated with H89 for 10 min prior to stimulation with 10-μg/ml PGI2 were analyzed for cell adhesion as described in the legend to Fig. 4A. (E) HUVECs untreated or pretreated with H89 for 10 min prior to stimulation with 10 μM FSK were analyzed for cell adhesion as described in the legend to Fig. 4D. For panels A to E, data are expressed as means ± standard deviations of the results from triplicate samples. Similar results were obtained in at least three independent experiments. Significant differences between two groups determined by Student's *t* test are indicated by a single asterisk ($P < 0.05$) or double asterisks ($P < 0.01$). (F) HUVECs serum starved in 1% BSA-containing medium 199 for 6 h, followed by pretreatment with (+) or without (−) 5 μM H89 for 10 min, were stimulated with vehicle and 10 μM FSK for 10 min. Phosphorylation of CREB was assessed by Western blot analysis with anti-CREB (CREB) and anti-phospho-CREB-specific (pCREB) antibodies.

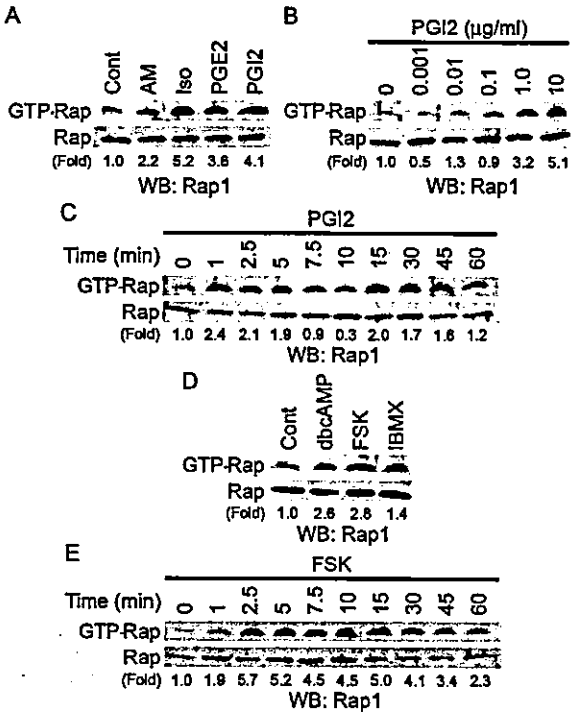

FIG. 6. cAMP induces Rap1 activation. (A) Serum-starved HUVECs kept in medium 199 containing 1% BSA overnight were stimulated with cAMP-elevating agonists for 2.5 min as indicated at the top and at the concentrations described in the legend to Fig. 1A. GTP-bound Rap1 was detected by pull-down assay as described in Materials and Methods. Activation indicates the ratio of the poststimulation GTP-Rap1 intensity of total Rap1 intensity to the prestimulation GTP-Rap1 intensity of total Rap1 intensity. (B) Rap1 activation was analyzed by detecting GTP-bound Rap1 with lysates from HUVECs stimulated with PGI2 for 2.5 min at the different concentrations indicated at the top. (C) Rap1 activation was analyzed by detecting GTP-bound Rap1 with lysates from cells stimulated with 10-μg/ml PGI2 for the time period indicated at the top. (D) Serum-starved HUVECs similar to those described in the legend to panel A were stimulated with the reagents indicated at the top for 10 min at the same concentrations described in the legend to Fig. 1A. Rap1 activation was assessed by a method similar to that described for panel A. (E) The effect of 10 μM FSK on time-dependent Rap1 activity was examined as described for panel C. Representative results from at least three independent experiments are shown for all panels.

8-CPT-2′-O-Me-cAMP dramatically reduced basal endothelial permeability, as did FSK and dbcAMP (Fig. 7B). Thrombin-induced permeability was also inhibited by 8-CPT-2′-O-Me-cAMP (Fig. 7C). Furthermore, we examined the effect of 8-CPT-2′-Me-cAMP on in vivo vascular permeability. VEGF-induced vascular permeability was completely blocked by coinjection of 8-CPT-2′-O-Me-cAMP (Fig. 7D). In addition, adhesion

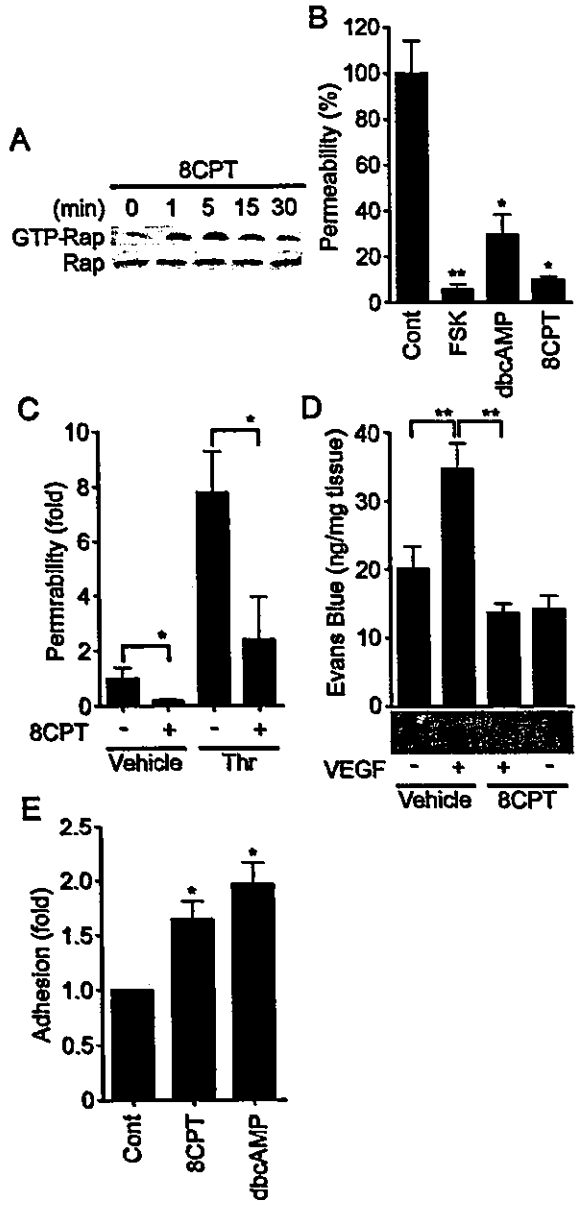

FIG. 7. Activation of Epac is sufficient to enhance VE-cadherin-dependent cell adhesion and endothelial barrier function. (A) Serum-starved HUVECs in medium 199 containing 1% BSA were stimulated with 0.2 mM 8-CPT-2'-O-Me-cAMP (8CPT) for the indicated time. Rap1 activity was determined as described in the legend to Fig. 6A. The result is a representative from three independent experiments. (B) Permeability of cells treated with the reagents as indicated on the bottom for 30 min was analyzed as described in the legend to Fig. 1A. (C) The effect of 0.2 mM 8CPT-2'-O-Me-cAMP on 2-U/ml thrombin-induced permeability was analyzed as described in the legend to Fig. 1B. (D) Effect of 8CPT-2'-O-Me-cAMP on VEGF-induced permeability was assessed by intradermal Miles assay as described in Materials and Methods. Amounts of extravasation of Evan blue in mouse dermal skin were measured 60 min after intradermal injection of vehicle and VEGF together with (+) or without (−) 8CPT. Mean leakage ± standard deviation of the results from 6 mice per group is expressed as nanograms of weight of extravasated Evans blue per milligram of weight of dermal skin. A photograph on the bottom shows leakage of Evans blue in dermal skin. (E) HUVEC adhesion to the VEC-Fc-coated dish in the presence of 0.2 mM 8CPT and 1 mM dbcAMP for 7 min was analyzed as described in the legend to Fig. 4F. In panels B, C, and E, data are expressed as means ± standard deviations of the results from triplicate samples. A significant difference from the control in panels B and E or between two groups in panels C and D was determined by Student's t test and indicated by a single asterisk ($P < 0.05$) or double asterisks ($P < 0.01$).

of HUVECs to the VEC-Fc-coated dish was significantly enhanced by 8-CPT-2'-O-Me-cAMP (Fig. 7E). Hence, Epac activation is sufficient to enhance VE-cadherin-dependent cell adhesion and to augment endothelial barrier function in vitro and in vivo.

Rap1 activation is essential for VE-cadherin-dependent cell adhesion and endothelial barrier function. We next proceeded to investigate the role of Rap1 in VE-cadherin-dependent cell adhesion and endothelial barrier function. To examine the effect of Rap1 on cell permeability and VE-cadherin-mediated cell adhesion, we inactivated endogenous Rap1 by adenovirus-expressing Rap1GAPII (Ad-RapGAP), which specifically catalyzes the hydrolysis of GTP to GDP on Rap1 (30). As shown in Fig. 8A, endogenous Rap1 activity was almost completely suppressed by the expression of increasing amounts of Rap1GAPII in HUVECs. This Rap1 inactivation paralleled the increase in basal permeability (Fig. 8B) and the inhibition of cell adhesion to the VEC-Fc-coated dish (Fig. 8D). In contrast, a constitutively active Rap1, Rap1V12, reduced both basal and thrombin-increased cell permeability (Fig. 8C). VE-cadherin-mediated cell adhesion was also enhanced by Rap1V12 and EpacΔcAMP, a constitutively active mutant of Epac (Fig. 8D). Taken together, these results indicate that Rap1 activation is required for VE-cadherin-mediated cell adhesion and endothelial barrier function.

cAMP enhances VE-cadherin-dependent cell adhesion and endothelial barrier function by activating Rap1. To test the requirement for Rap1 in endothelial barrier enhancement by cAMP-elevating GPCR agonists, we infected HUVECs with Ad-RapGAP and examined the effect of inactivation of Rap1 on PGI2- and FSK-induced reduction of cell permeability. Although basal endothelial permeability was reduced by PGI2 and FSK (Fig. 9A and B), overexpression of Rap1GAPII increased not only basal but also PGI2- and FSK-reduced endothelial permeability, indicating the requirement of Rap1 activity for PGI2- and FSK-induced barrier enhancement. We also investigated the involvement of Rap1 in PGI2- and FSK-induced VE-cadherin-dependent cell adhesion. PGI2 and FSK augmented VE-cadherin-dependent cell adhesion of HUVECs infected with control adenovirus (Ad-LacZ); however, their effects were dramatically suppressed by overexpression of Rap1GAPII (Fig. 9C and D). These data demonstrate that cAMP enhances VE-cadherin-dependent cell adhesion and endothelial barrier functions by activating Rap1.

cAMP induces endothelial cortical actin rearrangement in a Rap1-dependent manner. Endothelial barrier function is largely dependent upon the actin cytoskeleton supporting junctional adhesion molecules (10). Thus, we examined the effect of cAMP on cortical actin polymerization and assembly of polymerized actin in a monolayer of endothelial cells. Cortactin, an actin-binding protein, is known to be implicated in cortical actin rearrangement (8) and suggested to regulate S1P-induced endothelial barrier enhancement (11). PGI2,